Stony Brook University

Modeling Excitable Cells Using Hybrid Automata

A Dissertation Presented
by
Pei Ye

to
The Graduate School
in Partial Fulfillment of the
Requirements
for the Degree of
Doctor of Philosophy
in
Computer Science
Stony Brook University

August 2008

Stony Brook University
The Graduate School

Pei Ye

We, the dissertation committee for the above candidate for the degree of Doctor of Philosophy, hereby recommend acceptance of this dissertation.

Radu Grosu, Dissertation Advisor
Associate Professor, Computer Science Department

Scott A. Smolka, Chairperson of Defense
Professor, Computer Science Department

Emilia Entcheva
Associate Professor, Biomedical Engineering Department

Ira S. Cohen
Professor, Physiology and Biophysics Department

This dissertation is accepted by the Graduate School

Lawrence Martin
Dean of the Graduate School

Abstract of the Dissertation

Modeling Excitable Cells Using Hybrid Automata

by

Pei Ye

Doctor of Philosophy

in

Computer Science

Stony Brook University

2008

Hybrid automata are an increasingly popular modeling formalism for systems that exhibit both continuous and discrete behavior. Intuitively, a hybrid automaton is an extended finite-state automaton, the states of which encode the various phases of continuous dynamics a system may undergo, and the transitions of which are used to express the switching logic between these dynamics. Excitable cells are a good example of biologically inspired hybrid systems: trans-membrane ion fluxes and voltages may vary continuously but the transition from the resting state to the excited state is generally considered an all-or-nothing discrete response. In this work, we first show that two existing models of excitable cells fall into the hybrid automata framework. We then design a specific kind of hybrid automata: Cycle-Linear Hybrid Automata (CLHA), to model multiple physiological properties of excitable cells including action potential, restitution and hyper-polarization. Spatial simulation demonstrates that our model is 8 times faster than the traditional models. We present how machine learning techniques are applied to automatically learn the parameters of CLHA from existing data and how reachability analysis is used to verify critical conditions for the excitement of neurons. A formal analysis of abnormal excitation (early afterdepolarization) in cardiac tissue is also included. At last, a rational CLHA with more physiological details is presented.

Contents

List of Tables

List of Figures

Acknowledgements

This is a great opportunity to express my respect for Prof.Radu Grosu, Prof.Scott Smolka and Prof.Emilia Entcheva for their continuous encouragement and commitment in my doctoral work. They stimulated and helped me to develop analytical thinking, research skills and scientific writing throughout all these years, from which I shall benefit in my whole life.

I am also grateful for having Prof.Ira Cohen in my doctoral committee for his generous time, support and inspiring advices.

I'd like to thank the assistance and advice I received from Mike True, Sayan Mitra, Prof. Anita Wasilewska, Prof.IV Ramakrishnan and all my colleagues.

Finally, I'd like to thank my family: my parents and my sister for their constant support. I'm especially grateful to my husband, Yi, for helping me keep my life in proper perspective and balance.

This research is supported in part by NSF Grant CCF05-23863 and NSF CAREER Grant CCR01-33583.

Publications

1. P. Ye, R. Grosu, S.A. Smolka and E. Entcheva. **Formal Analysis of Abnormal Excitation in Cardiac Tissue**, *In Proc. of CMSB'08, the 6th International Conference on Computational Methods in Systems Biology, Rostock, Germany, October, 2008.*
2. P. Ye, E. Entcheva, S.A. Smolka and R. Grosu. **Symbolic Analysis of the Neuron**, *In Proc. of ICBBE'08, the 2nd International Conference on Bioinformatics and Biomedical Engineering, Shanghai, China, May, 2008.*
3. P. Ye, E. Entcheva, S.A. Smolka and R. Grosu. **A Cycle-Linear Hybrid-Automata Model for Excitable Cells**, *IET Systems Biology (SYB), vol. 2(1), pp. 24-32, January, 2008.*
4. R. Grosu, S. Mitra, P. Ye, E. Entcheva, IV Ramakrishnan and S.A. Smolka. **Learning Cycle-Linear Hybrid Automata for Excitable Cells**, *In Proc. of HSCC'07, the 10th International Conference on Hybrid Systems: Computation and Control, Pisa, Italy, April, 2007, pp. 245-258, Springer, LNCS 4416.*
5. P. Ye, E. Entcheva, S.A. Smolka, M.R. True and R. Grosu. **A Cycle-Linear Approach to Modeling Action Potentials**, *In Proc. of EMBS'06, the 28th IEEE International Conference of the Engineering in Medicine and Biology Society, New York City, USA, August, 2006, pp. 3931-3934, IEEE Press.*
6. P. Ye, E. Entcheva, S.A. Smolka, M.R. True and R. Grosu. **Hybrid Automata as a Unifying Framework for Modeling Cardiac Cells**, *In Proc. of EMBS'06, the 28th IEEE International Conference of the Engineering in Medicine and Biology Society, New York City, USA, August, 2006, pp. 4151-4154, IEEE Press*
7. M.R. True, E. Entcheva, S.A. Smolka, P. Ye and R. Grosu. **Efficient Event-Driven Simulation of Excitable Hybrid Automata**, *In Proc. of EMBS'06,*

the 28th IEEE International Conference of the Engineering in Medicine and Biology Society, New York City, USA, August, 2006, pp. 3150-3153, IEEE Press.

8. P. Ye, E. Entcheva, S.A. Smolka and R. Grosu. **Efficient Modeling of Excitable Cells using Hybrid Automata**, *In Proc. of CMSB'05, the 3rd International Workshop on Computational Methods in Systems Biology, Edinburgh, UK, April, 2005, pp. 216-227.*

Chapter 1

Introduction

1.1 Hybrid Automata

Hybrid automata are an increasingly popular modeling formalism for systems that exhibit both continuous and discrete behavior. Intuitively, a hybrid automaton is an extended finite-state automaton, the states of which encode the various phases of continuous dynamics a system may undergo, and the transitions of which are used to express the switching logic between these dynamics. Hybrid automata are well suited as a computational model for continuous-discrete systems as they possess an intuitive graphical representation, can be used in a natural way to achieve a piecewise, possibly linear, approximation of any nonlinear systems and facilitate formal analysis due to their automata-theoretic nature.

Traditionally, HA have been used to model embedded systems, including automated highway systems, [22, 60], air traffic management, [45, 47], embedded automotive controllers, [7], robotics, [5] and real-time circuits. [48].

1.1.1 Formal Definition

Intuitively, a **Hybrid Automaton** (HA) is an extended finite-state automaton, where each state is endowed with a continuous dynamics [35].

Formally, an HA $\mathcal{A} = (X, G, \mathit{init}, \mathit{inv}, \mathit{flow}, \mathit{jump}, \mathit{event})$ over finite set Σ of **events** is a 7-tuple, whose components are as follows:

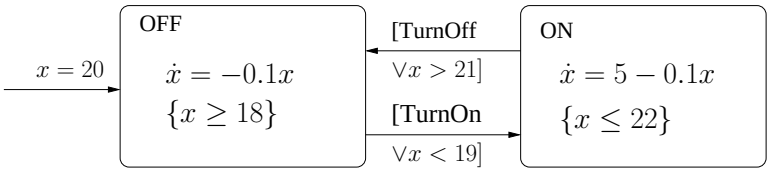

Figure 1: A thermostat system modeled as an HA.

- A finite set X of real-valued **variables** $x_1, \ldots, x_n$; their dotted form $\dot{x}_i \in \dot{X}$ represents first derivatives and their primed form $x_i' \in X'$ represents values at the conclusion of discrete steps (jumps); n is called the *dimension* of $\mathcal{A}$.
- A finite **control graph** $G = (V, E)$, where vertices in V are called *modes* and edges in E are called *switches*.
- For each mode $v \in V$, vertex-labeling functions *init*, *inv* and *flow* with domain V and range P, where P is the set of all logical predicates. Initial condition $init(v)$ and invariant $inv(v)$ are predicates with free variables from X. Flow $flow(v)$ is a predicate with free variables from $X \cup \dot{X}$ representing a set of ordinary (partial) differential (in)equalities.
- A finite set Σ of **events** which are essentially binary variables controlled from outside the system, and an edge-labeling function $event : E \to \Sigma$ that assigns to each switch an event.
- Edge-labeling functions $jump: E \to (Guard, Action)$ where *Guard* is the set of predicate with free variables from $X \cup \Sigma$ and *Action* is the set of assignments that update the variables in X'.

Intuitively, $\mathcal{A}$ spends time in its modes $v \in V$, where it updates its variables according to the flow predicate $flow(v)$. Jumps $jump(e)$ on switches $e = (v, w)$ are in contrast instantaneous, where v is the beginning mode and w is the end mode of the switch. A jump on e is taken whenever the jump's guard $jump(e).guard$ is enabled for the current values of variables X, or the invariant of the current mode $inv(v)$ is unsatisfied.

An HA has a natural graphical representation as a state-transition diagram, with control modes as the states and control switches as the transitions. Flows and invariants (predicates within curly braces) appear within control modes, while jump conditions (in square brackets) and actions appear near the control switches.

We shall use lower-case Roman letters, such as x, y, v, and possibly v_x, v_y, etc., to denote continuous variables.

For example, let $\mathcal{A}$ be the HA of Figure 1, which models a simple thermostat system. $\mathcal{A}$ is of dimension 1 with $X = \{x\}$, where x represents the current temperature. Also, $G = (\{ON, OFF\}, \{(ON, OFF), (OFF, ON)\})$, $inv(OFF) = \{x \geq 18\}$, $inv(ON) = \{x \leq 22\}$, $flow(OFF) = \{\dot{x} = -0.1x\}$, $flow(ON) = \{\dot{x} = 5 - 0.1x\}$, $jump((OFF, ON)).Guard = \{TurnOff \vee x > 21\}$, $jump((ON, OFF)).Guard = \{TurnOn \vee x < 19\}$, $\Sigma = \{TurnOn, TurnOff\}$, $event((OFF, ON)) = TurnOn$,$event((ON, OFF)) = TurnOff$. Initially, $\mathcal{A}$ is in mode `OFF` with x initialized to 20°C. While in this mode, the heater is off and the temperature drops. It switches to mode `ON` when either: (i) the event *TurnOn* occurs, signifying that the heater has been manually turned on; or (ii) the temperature falls below 19°C, but not below 18°C(when the system is forced to leave mode `OFF`). In mode `ON`, the heater is on and the temperature rises. It switches to mode `OFF` when event *TurnOff* is true or the temperature rises above 21°C, but not above 22°C.

Hybrid automata are in general *nondeterministic* in that their mode switching times are nondeterministic. For example, consider the HA of Figure 1. In the absence of event *TurnOn*, it may switch from mode `OFF` to `ON` any time during the temperature range $18 \leq x < 19$. We found, however, that, for the modeling of excitable cells, nondeterminism is not required. That is, their behavior can be captured by HAs whose mode switching times are uniquely determined. We also found it sufficient to consider HAs whose flows are defined by differential equalities (i.e. equations), rather than inequalities. Therefore, although nondeterminism and differential inequalities in flow definitions are important HA modeling features, we shall not consider them further in this report.

Linear Hybrid Automata By restricting the form of flow functions in the modes of HAs (as long as other conditions), we can classify HAs according to their expressiveness power. One of them we are particularly interested is called Linear Hybrid Automata. The definition is given below.

An HA is a **linear HA (LHA)** if it has the following properties:

- **Linear flows**. Every $flow(v)$ is a linear time-invariant differential equation of the form $\dot{X} = AX + BU$, where A is a constant $n \times n$ matrix, B is a constant

scalar, and U is an input vector of dimension $n \times 1$ that ranges inside a convex polyhedron.

- **Linear invariants and guards**. The variable spaces that make $inv(v)$ and $jump(e).Guard$ true also form convex polyhedra.

1.1.2 Reachability Analysis

The appealing point of HA models is that, on one hand, HA can be used to model complex dynamic behavior which is traditionally modeled in ordinary differential equation (ODE) or partial differential equation (PDE) systems; on the other hand, it allows formal analysis carried out. We want to develop HA models to utilize its analytical power to help us have a better understanding of the target system. The most studied analysis on HA is called reachability analysis.

The reachability problem for HA is stated as follows: *Will the system, subject to certain initial conditions, ever enter an "unsafe" state?* The problem is in general undecidable; however, under certain restrictions on the HA flows or jumps, it becomes decidable [6].

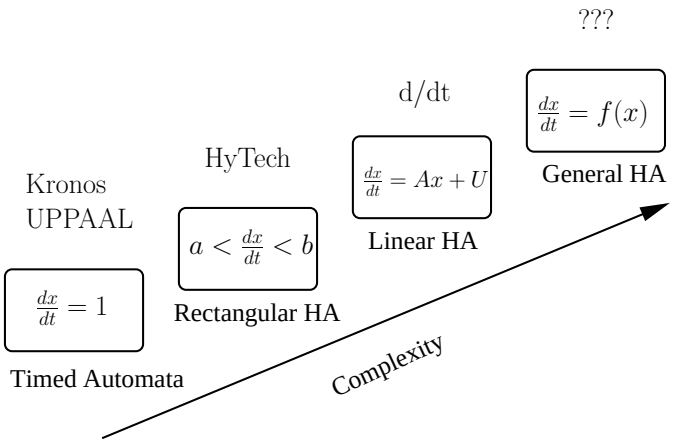

Figure 2: The complexity of different subclasses of HA

Figure 2 illustrates the increasing complexity (in terms of the flows) of the reachability problem for different subclasses of HA. Timed Automata (TA) [4] have the simplest form of flow function: the only continuous variables are clocks whose derivative is one, and clocks can be reset on transitions. Existing tools for TA

include UPPAAL [10] and Kronos [64]. Initialized, rectangular hybrid automata (RA) [36] generalize the class of TA by allowing non-clock state variables whose flow functions are differential inclusions of the form $a \leq dx/dt \leq b$, where a and b are integer constants. The prevalent tool for RA is HyTech [34]. O-minimal hybrid automata (OA) restrict the jumps but allow O-minimal structures for the flows [43]. In particular, HA with linear differential equations (LHA) are in the class OA, and therefore their reachability problem is decidable [6]. A popular tool for LHA is d/dt [20].

In this report, we will present a preliminary result of reachability analysis of the excitation of neuron. The analysis successfully shows the input current serves as a bifurcation parameter in the system.

1.2 An Introduction to Excitable Cells

1.2.1 Action Potential

Excitable cells include neurons, cardiac cells, skeletal, and smooth muscle cells. For cardiac cells, on each heart beat, an electrical control signal is generated by the sinoatrial node, the heart's internal pacemaking region. Electrical waves then travel along a prescribed path, exciting cells in the main chambers of the heart (atria and ventricles) and assuring synchronous contractions. At the cellular level, the electrical signal is a change in the potential across the cell membrane which is caused by different ion currents flowing through the cell membrane. This electrical signal for each excitation event is known as an **action potential** (AP). Figure 3 shows the AP waveform for a guinea-pig ventricular cell.

For non-pacemaking excitable cells, APs are externally triggered events: a cell fires an action potential as an all-or-nothing response to a supra-threshold stimulus, and each AP follows the same sequence of phases and maintains approximately the same magnitude regardless of the applied stimulus. After an initial step-like increase in the membrane potential, an AP lasts for a couple of milliseconds to hundreds of milliseconds in most mammals. During an AP, generally no re-excitation can occur. The early portion of an AP is known as the "absolute refractory period" due to its non-responsiveness to further stimulation. The later portion is known as

the “relative refractory period”, during which an altered secondary excitation event is possible if the stimulation strength or duration is raised.

1.2.2 Restitution

When an excitable cell is subjected to repeated stimuli, two important time periods can be identified: the **action potential duration** (APD), the time the cell is in an excited state, and the **diastolic interval** (DI), the time between the end of the action potential and the next stimulus. Figure 3 illustrates the two intervals. The function relating APD to DI with change in stimulation frequency is called the APD **restitution function**. As shown in Figure 4, the relationship is nonlinear and captures the phenomenon that a longer recovery time is followed by a longer APD. A physiological explanation of a cell’s restitution is rooted in the ion-channel kinetics as a limiting factor in the cell’s frequency response. The sum of the APD and DI is called the **Basic Cycle Length** (BCL).

The **S1S2 protocol** is often used to determine the restitution function of an excitable cell. In this protocol, a cell is driven into a stable mode, in which a stable APD may be observed, by first subjecting it to a train of so-called S1 stimuli at a fixed BCL. Immediately thereafter, a single S2 stimulus, having a different (i.e. shorter) BCL is delivered. As such, one can associate a DI-APD pair with each running of the protocol, viz. the DI preceding the S2-induced APD. By repeating this procedure and varying the DIs before S2, one gradually constructs the graph of the restitution curve.

1.2.3 Hyper-Polarization

In cardiac cells, where repolarization phase is relatively long (lasting for several hundreds milliseconds), hyper-polarization is the phenomenon that when the cell is under negative stimulation (opposite direction to the stimulation for an AP) during repolarization, the membrane voltage will be first brought down (more negative), then go back to the original value if the stimulation is small; or return to resting if the stimulation is large. Fig. 5 shows hyper-polarization of guinea pig ventricular cells. The figure is generated by superposition of different curves produced by using different stimulation currents. The stimulation happens at 40ms later

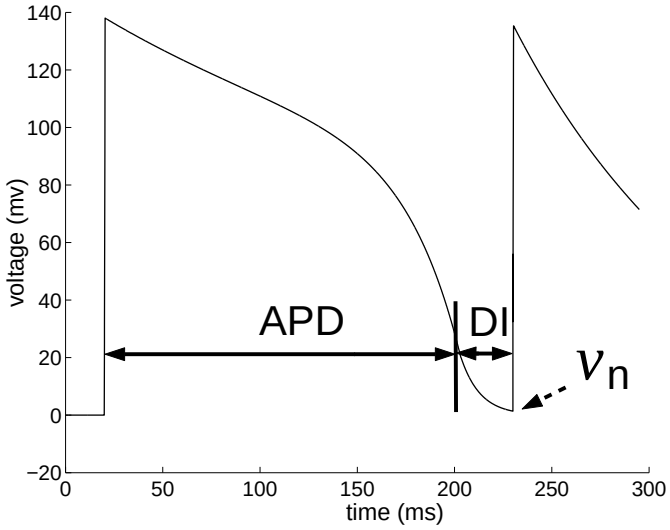

Figure 3: The AP and its APD and DI time periods.

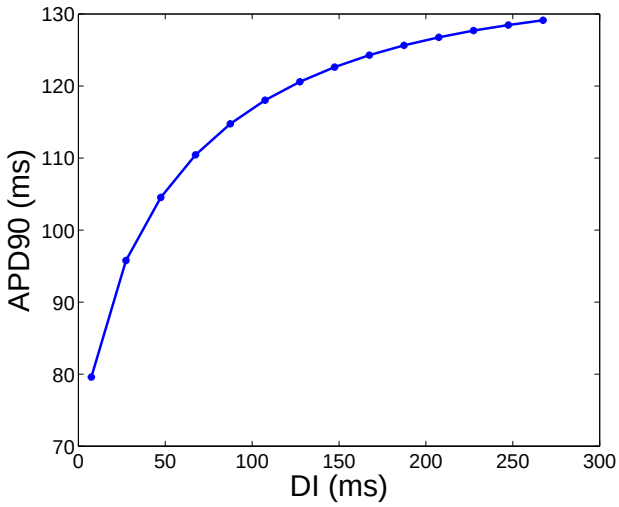

Figure 4: APD dependence on DI in LRd model.

than the beginning of AP and the stimulation currents range from 0 to $-200\mu A/cm^2$. We can see that when current is small, at the end of stimulation, AP curve jumps

back the original curve while when current increases, AP is brought back to the resting phase.

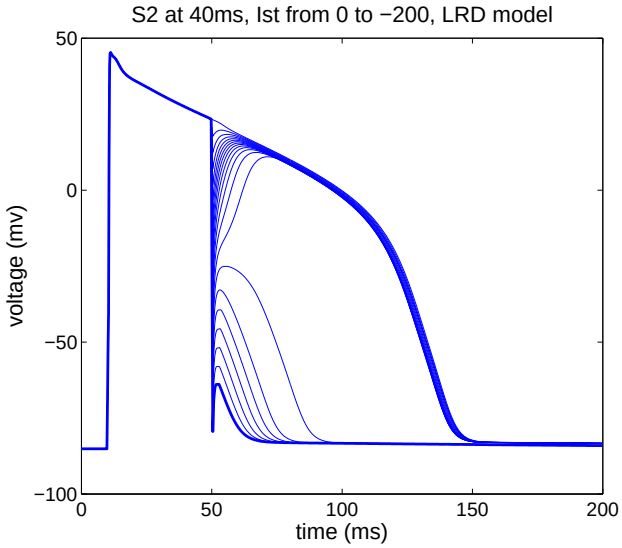

Figure 5: Hyper-Polarization of cardiac cells.

1.2.4 Action Potential Propagation

The most interesting property of excitable cells is not the single cell behavior, but the propagation of AP in the excitable cell tissues. The propagation of AP in neurons causes the passing of information in different components of nerve system while the propagation of AP in cardiac cells causes the cardiac muscle contraction, which pumps blood into body. However, the modeling of propagation process is relatively independent from the modeling of single cells. The single cell model is usually consisted of a set of ordinary differential equations (ODEs) together with a Laplace operator which calculates the diffusion factor of the overall currents during the propagation. The single cell model provides a simple interface (the membrane voltage and the overall current, for example) to the propagation model and they have to be coupled to do tissue simulation in 2D or organ simulation in 3D.

In a healthy heart, the propagation of AP will look like a normal wave. Under

rare situations, the wave change into a spiral shape. If this happen, heart will fail to contract, causing fatal consequences. The simulation of this spiral wave or reentry wave is thus becoming an important aspects of cardiac cell research.

In this work, we have not studied the modeling of the propagation process in HA. Instead, we embed our single cell model into a software tool which implements a popular propagation model and run the resulting model to simulate the generation of spiral waves. The result is presented in later chapters.

1.3 Related Work

1.3.1 Traditional Modeling Methods for Excitable Cells

1.3.1.1 ODE and PDE Systems

Modeling of the ionic processes that underlie cell excitation dates back to 1952, when Hodgkin and Huxley formulated their model of the squid giant axon [38]. Intuitively, the Hodgkin-Huxley (HH) model is that of a nonlinear resistor-capacitor (RC) circuit with current sources, defining AP in terms of a stimulation current and three ionic currents: (fast) inward sodium, (slow) outward potassium, and a time-independent linear (leak) current. The ionic currents depend themselves on the AP via a gating mechanism (a time-varying conductance). The corresponding nonlinear system of equations is given below, where: V, m, n and h are continuous state variables; V is the AP, m, n and h are the ion-channel gates; $\overline{g}_{\mathrm{Na}}$,$\overline{g}_{\mathrm{K}}$,$\overline{g}_{\mathrm{L}}$ are the constants which represent the maximum channel conductances for the sodium, potassium and leakage channel, respectively; E_{Na},E_{K},E_{L} are the constants for reversal potentials for these channels; m_∞, h_∞ and n_∞ are the ion-channel gates' steady-state values, and τ_m, τ_h and τ_n are their time-constant values; C is the constant cell capacitance and I_{st} is the stimulation current.

$$C\dot{V} = -\overline{g}_{\mathrm{Na}} m^3 h (V - E_{\mathrm{Na}}) - \overline{g}_{\mathrm{K}} n^4 (V - E_{\mathrm{K}}) - \overline{g}_{\mathrm{L}} (V - E_{\mathrm{L}}) + I_{\mathrm{st}}$$

$$\begin{array}{llll} \tau_m & \dot{m} = m - m_\infty & \tau_m = 1/(\alpha_m + \beta_m) & m_\infty = \alpha_m/(\alpha_m + \beta_m) \\ \tau_h & \dot{h} = h - h_\infty & \tau_h = 1/(\alpha_h + \beta_h) & h_\infty = \alpha_h/(\alpha_h + \beta_h) \\ \tau_n & \dot{n} = n - n_\infty & \tau_n = 1/(\alpha_n + \beta_n) & n_\infty = \alpha_n/(\alpha_n + \beta_n) \end{array}$$

$$\alpha_m(V) = \frac{2.5-0.1V}{e^{2.5-0.1V}-1} \quad \alpha_h(V) = 0.07e^{-\frac{V}{20}} \quad \alpha_n(V) = \frac{0.1-0.01V}{e^{1-0.1V}-1}$$
$$\beta_m(V) = 4e^{-\frac{V}{18}} \quad \beta_h(V) = \frac{1}{e^{3-0.1V}+1} \quad \beta_n(V) = 0.125e^{-\frac{V}{80}}$$

The HH model with its 3 membrane currents, 4 state variables, and 12 fitted parameters laid the foundation for subsequent models of excitable cells of increasing complexity. All of these models use multiple continuous state variables (voltage, ion-channel gates, ion concentrations) to describe action potential in different cell types. One of the most popular cardiac-cell models is the dynamic Luo-Rudy model [46]. The LRd model uses 11 different membrane currents, more than 20 state variables and over 150 fitted parameters to describe the AP. Due to space constraints, the full structure of the LRd model is not listed here.

The single cell AP is usually modeled in ODE systems. When taking consideration of the diffusion factor in the cell network, a Laplace operator is added when calculating the overall membrane currents. Thus the tissue or organ simulation is conducted on a large PDE systems.

1.3.1.2 Cellular Automata

While PDE systems are inefficient to run large-scale simulations and impossible to analyze, people found **Cellular Automaton** (CA) as an alternative. A CA is a pure discrete system which is consisted of a cell grid, where a cell can have several state and all of them must follow the same rules to update according to the neighboring cell states.

The limitation of CA is due to the fact that though it is efficient, the result is quite qualitative rather than quantitative. It may lose too much information for a real world problem, especially in the clinical studies.

1.3.2 Application of hybrid automata to Excitable cells

Recently, hybrid automata have been used to model and analyze biological systems, such as cellular cycles and immune response [8], bio-molecular networks [2], gene-regulatory networks [21, 44, 56], protein-signaling pathways [29], and metabolic processes [11]. The hybrid-system metaphor has also been used to

develop algorithms for large-scale simulation of biological systems [42]. Biological systems are intrinsically hybrid in nature: biochemical concentrations may vary continuously, yet discrete transitions between distinct states are also possible.

Once an HA model has been developed for a biological system, it can be used to explore the system's parameter space. Moreover, because of their abstract nature (relative to nonlinear systems), HA admit the possibility of formal systems analysis. Of particular interest for dynamical systems are *reachability* and *stability* analysis. The former allows one to check whether the transient behavior of an HA contains undesired modes of operation [3, 29]. The latter allows one to check if the HA, in steady state, exhibits unstable (or chaotic) behavior [12, 23]. The information gleaned from these forms of analysis can be exploited to *control* the system in question such that it stays within desired limits.

Excitable cells are another good example of such hybrid systems - transmembrane ion fluxes and transmembrane voltage may vary continuously but transition from resting to excited state is generally considered all-or-nothing discrete response. Fig. 6 shows this behavior. (The data is from Hodgkin-Huxley model.) As the increase of stimulation current, the status of the cell changes from *failed initialization* to *full AP* without intermediate state. This is easily transformed to a hybrid system with two modes, where the switch from one mode to another depends on whether the input exceeds the threshold value.

Similar bifurcation behavior can be found in the hyper-polarization phase as well, as Fig. 5 illustrated.

Explicit Application EC excitation is a less studied area of HA application than the other applications mentioned above. The major reason is that the dynamics of AP is highly nonlinear, and model would become meaningless if AP is abstracted away.

The closest work we are aware of is Dumas and Rondepierre [23]. They started from Hodgkin-Huxley (HH) model, which is a 4-variable nonlinear system. First through order-reduction, they eliminated 2 variables and derived a 2-state nonlinear system; then by studying the phase portraits, they used piecewise linear functions to approximate the nonlinear functions of each state equation; at last, they studied bifurcation of the system through phase-space plotting. Though their work provided

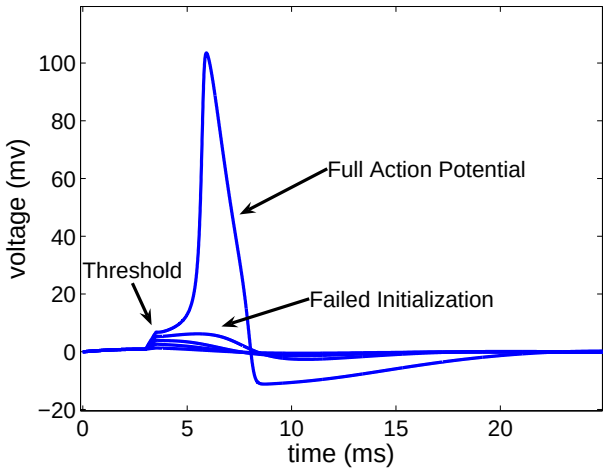

Figure 6: All-Or-Nothing response of action potential of neuron.

a way to analyze the original nonlinear system, it is less extensible than our method and we will show that the same bifurcation result can be derived through a totally automatic reachability analysis on the HA constructed for the HH model in a later chapter.

Implicit Application through the Use of Heaviside Function The similar idea that using piecewise linear function to approximate the original nonlinear system has been adopted by many researchers in the cell modeling area when they simplify the detailed PDE systems. This usually entails substitution of the fast-transitioning continuous functions with a **Heaviside function**.

Even though those models constructed using Heaviside functions did not use word “Hybrid” explicitly, we found it can be rewritten into HA framework equivalently. In Chapter 2, we can see that some popular simplified models which adopted the above idea are safely transformed into HA framework, showing the generality of HA models.

Chapter 2

Hybrid Automata as a Unifying Framework for Modeling Excitable Cells

During the early stages of the quest for models of excitable cells amenable to analytical investigation, FitzHugh and Nagumo proposed an approximate model of excitable cells [26], referred to here as the FHN model. With their model, they showed that a modified version of the Van der Pol oscillator with two state variables can mimic the essential features of the Hodgkin-Huxley dynamics.

Subsequently, a piecewise-linear version of the FHN model was proposed by McKean [49] which used a **Heaviside function** to represent switches between linear regimes or modes. Since then, the Heaviside function has been used in different simplified renditions of excitable-cell models to achieve piecewise control.

In this chapter, we first show how a dynamic system with Heaviside function turns into a hybrid automaton, then rewrite two widely accepted models into hybrid automata framework.

2.1 From Heaviside Control to Hybrid Automata

Discrete transitions in system behavior, such as those captured by Heaviside functions, are an integral part of the HA formalism. Let S be a dynamic system

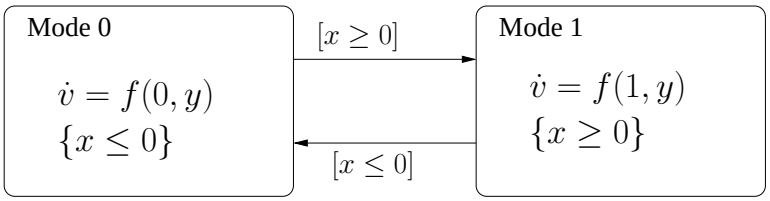

Figure 7: Heaviside function recast as an HA.

defined using the Heaviside function. We present a systematic way to transform *S* into an equivalent HA. The Heaviside function $H(x)$ is a discontinuous function defined as follows:

$$H(x) = \begin{cases} 0, & x < 0; \\ 1, & x \geq 0. \end{cases} \tag{1}$$

Assuming that the state equation of *S* has the structure of Equation (2), where $\vec{v}$ is a vector of state variables and which is *x*, it is straightforward to show that *S* is equivalent to the HA of Figure 7.

$$\dot{v} = f(H(x), y), \quad \vec{v} = (x, \vec{y}) \tag{2}$$

One can generalize the above translation to any dynamic system whose state equations are defined using Heaviside functions. In the following, we apply this translation to two recently proposed approximate models for cardiac-tissue excitability: the piecewise-linear model of Biktashev [14] and the nonlinear model of Fenton and Karma [25].

2.2 Biktashev's Model

The increasing complexity of excitable-cell models describing AP morphology with large sets of state variables and nonlinear differential equations triggered continuous efforts to obtain simplified descriptions that preserve important properties.

Biktashev made the observation that the widely used FHN model is not sophisticated enough to capture the propagation failure due to dissipation of the wavefront,

a phenomenon seen in more realistic models [14]. This was attributed to the more phenomenological nature of the FHN model, which was not directly derived from the original HH model, but rather devised to mimic its properties. Instead, a formal derivation procedure was proposed based on singular perturbation theory developed by Tikhonov and Pontryagin [54, 58]. The procedure reduces the size of the differential equations by taking advantage of the fast-slow nature of the system; i.e. by separating the state variables into two groups, fast-slow, and by linking the two sets of equations via a perturbation parameter. The model thus obtained was able to overcome the above-mentioned deficiency of the original FHN model. Furthermore, its simplicity allowed analytical treatment [14, 15, 57].

Consider Biktashev's simplified model [14] below, where H is the Heaviside function, E is the transmembrane voltage, h is the probability density of a sodium-channel gate being open, D is the (constant) diffusion coefficient, and τ is also constant. $\dot{E}$ and $\dot{h}$ are the time derivatives of state variables E and h, and $\nabla(D\nabla E)$ is the second-order directional derivative on the 2-D space, representing the diffusion factor when modeling the spatial propagation of cell excitations.

$$\dot{E} = \nabla(D\nabla E) + H(E-1)h \tag{3}$$

$$\dot{h} = \frac{1}{\tau}(H(-E) - h) \tag{4}$$

From the prespective of one cell, $\nabla(D\nabla E)$ is the (input) stimulation current I_s produced by neighboring cells. Hence, equation (3) can be rewritten as follows: $\dot{E} = I_s + H(E-1)h$. Applying the transformation process for systems employing Heaviside control (see the previous subsection) yields the 3-mode HA of Figure 8, with each mode having flows described by linear time-invariant (LTI) differential equations.

The linearity of the flows is clearly an advantage of this model, as it supports efficient simulation and detailed analysis. However, the simplicity of Biktashev's model comes at a price: the inability to faithfully reproduce AP morphology, as discussed in [14, 15]. This is probably due to the treatment of τ as a constant, when in reality it is a voltage-dependent parameter that can vary over a relatively wide range. Recently, this piece-wise linear formulation has been augmented with

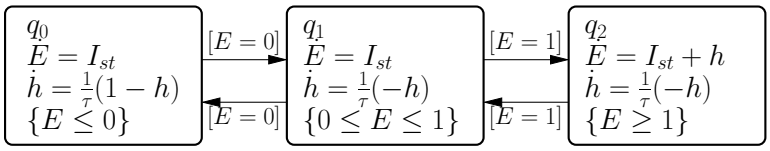

Figure 8: Biktashev's model in the HA framework.

non-Tikhonov asymptotic reduction to obtain a more realistic AP morphology. For example, Biktashev started with the Courtemanche model of the atrial heart cell [18] and applied asymptotic embedding, considering fast and slow variables, to obtain a reduced system [15, 55]. The resultant model captures AP morphology well, but is non-linear in each of the modes separated by a Heaviside function.

2.3 The Fenton-Karma Model

In [25], Fenton and Karma proposed a three-variable ionic model as a substitute for the full ionic LRd-type models, by grouping the various ion currents into three generic ones: fast inward current I_{fi}, slow inward current I_{si}, and slow outward current I_{so}. The corresponding three-variable model given below (Equations 5-11) contains dynamic functions for the normalized membrane voltage u, inactivation-reactivation gate v for I_{fi}, and gate w for I_{si}:

$$\dot{u} = \nabla \cdot (\widetilde{D}\nabla u) - J_{fi}(u;v) - J_{so}(u) - J_{si}(u;w) \tag{5}$$

$$\dot{v} = H(u_c - u)(1-v)/\tau_v^-(u) - H(u-u_c)v/\tau_v^+ \tag{6}$$

$$\dot{w} = H(u_c - u)(1-w)/\tau_w^- - H(u-u_c)w/\tau_w^+ \tag{7}$$

$$J_{fi}(u;v) = -\frac{v}{\tau_d}H(u-u_c)(1-u)(u-u_c) \tag{8}$$

$$J_{so}(u) = \frac{u}{\tau_o}H(u_c-u) + \frac{1}{\tau_r}H(u-u_c) \tag{9}$$

$$J_{si}(u;w) = -\frac{w}{2\tau_{si}}(1+tanh[k(u-u_c^{si}]) \tag{10}$$

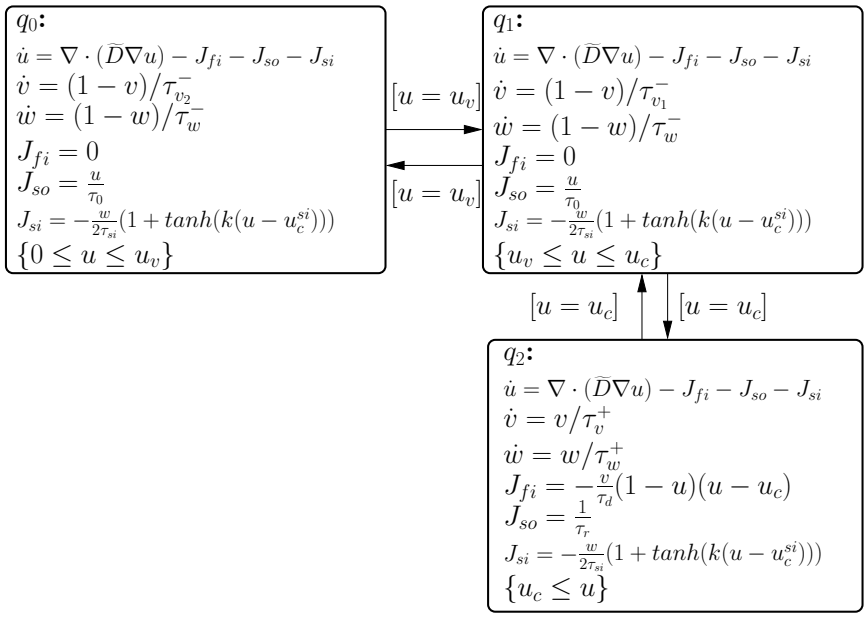

Figure 9: HA for the Fenton-Karma 3-variable, 3-ion-current model.

where $J_{fi}(u;v)$, $J_{si}(u;w)$, and $J_{so}(u)$ are the normalized versions of $I_{fi}(u;v)$, $I_{si}(u;w)$ and $I_{so}(u)$, respectively; u_c and u_c^{si} are the thresholds for activation of I_{fi} and I_{si}; τ_v^+, τ_w^-, τ_w^+, τ_d, τ_o, τ_r, and τ_{si} are time constants.

$$\tau_v^-(u) = H(u-u_v)\tau_{v_1}^- + H(u_v-u)\tau_{v_2}^- \tag{11}$$

$\tau_v^-(u)$ is further defined by the Heaviside function of Equation (11), where u_v is the threshold potential and $\tau_{v_1}^-$, $\tau_{v_2}^-$ are time constants.

The Fenton-Karma model recast as an HA is shown in Figure 9, where the HA was derived by taking into account the definition of the Heaviside functions.

The Fenton-Karma model has the flexibility to match AP morphology by correct selection of the parameters, possibly via an optimization procedure. It also has been shown to properly model restitution properties of other more complex models or empirically obtained data. However, similar to Biktashev's asymptotically reduced models, the resultant simplified system is still nonlinear and therefore not particularly well suited to analytic treatment.

Chapter 3

Modeling Excitable Cells Using Cycle-Linear Hybrid Automata

In the previous chapter, we saw that computational models of excitable cells employing the Heaviside function for discrete control can be recast as an HA. In particular, Biktashev's simplified model [14] corresponds to an LTI-HA: an HA having linear time-invariant (LTI) flows in each mode. An LTI-HA, such as Biktashev's, is amenable to efficient numerical (or event-driven [59]) simulation as well as formal analysis. Biktashev's simplified model and the corresponding HA are, however, unable to faithfully capture AP morphology.

Biktashev's more sophisticated models and the Fenton-Karma model correspond to HA having nonlinear flows in at least one mode, and faithfully capture AP morphology and restitution properties. Due to the nonlinearity present in these models, however, HA simulation is less efficient and powerful analysis techniques developed for linear systems are not directly applicable.

Given this state of affairs, we propose Cycle-Linear Hybrid Automata (CLHA) as a new HA-based formalism for modeling excitable cells. The CLHA formalism was designed to be both (i) abstract enough to admit formal analysis and efficient simulation; and (ii) expressive enough to capture the AP morphology and restitution properties exhibited by classical, nonlinear excitable-cell models (HH, LRd, and NNR, in particular).

The basic idea behind the CLHA model is the observation that, during an action potential, an excitable cell *cycles* through four basic modes of operation—resting, stimulated, upstroke, early repolarization, plateau, final repolarization—and the dynamics of each mode is essentially linear and time-invariant (LTI). Thus, on a per-cycle basis, a CLHA can be viewed as an LTI-HA. To capture possibly nonlinear, frequency-dependent properties such as restitution, the CLHA model is equipped with a one-cycle memory of the cell's voltage—in particular, the value of the cell's voltage when it was last subjected to an outside stimulus—and the per-mode parameters of the current cycle's LTI system of differential equations are updated according to this voltage. Consequently, the model's behavior is linear in any one cycle but appropriately nonlinear overall.

3.1 CLHA Derivation Method

The method we used to derive the CLHA model for excitable cells focuses on the following three issues:

Topology The topology of a CLHA refers to the design of its control graph; i.e. the control graph's modes and switches.

Flows Let $\mathcal{A}$ be a CLHA defined over a set (vector) of state variables X. The dynamics of $\mathcal{A}$ is determined by the dimension of X and, for each mode q of $\mathcal{A}$, the form of q's flow (system of ODEs in X).

Adaptability This refers to the mechanism built into the CLHA model that allows it to exhibit stimulation-frequency adaptability. This feature is essential for the successful modeling of AP morphology and restitution.

The discussion of our derivation method proceeds as follows. We first consider topology and flows, and in the process derive an LTI-HA model $\mathcal{A}_1$ that approximates the AP trajectory of one representative AP cycle of an excitable cell. Since for one AP cycle we are able to use LTI flows in each mode, $\mathcal{A}_1$ is an LTI-HA. We then turn our attention to adaptability. In the process, we derive our final CLHA model $\mathcal{A}_2$, which offers an accurate approximation of the (infinite-trajectory) phase

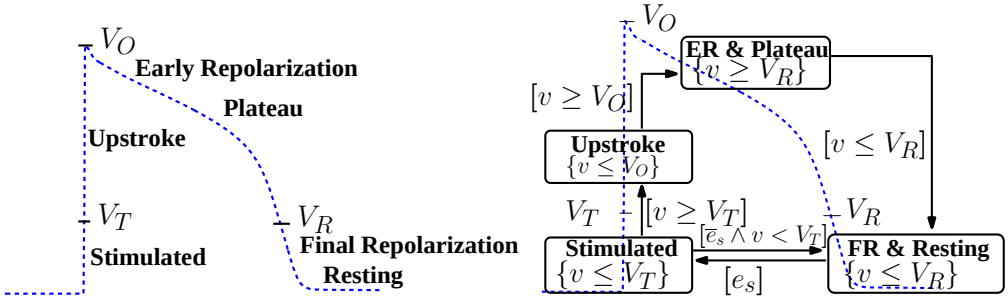

Figure 10: (a) Major AP phases. (b) Structure of the CLHA model.

space of the original nonlinear system by introducing a memory unit into LTI-HA $\mathcal{A}_1$. Finally, we give the formal definition of the CLHA model.

3.1.1 Topology

The choice of modes for both our LTI-HA $\mathcal{A}_1$ and CLHA $\mathcal{A}_2$ models is inspired by the fact that, although the AP for different cell types (neuron, cardiac myocyte, etc.) or different species (guinea pig, neonatal rat, etc.) exhibit different waveforms, when observed over time, one can universally identify the following phases within a cycle: **resting**, **upstroke**, **early repolarization**, **plateau or later repolarization**, and **final repolarization**. Figure 10(a) shows a typical AP cycle for a guinea pig ventricular cell. The voltage thresholds V_T, V_O and V_R serve to delineate one phase of the AP cycle from another.

For the purpose of mode identification, we are also interested in the period of time when an excitable cell is stimulated and can be further subjected to external stimulation. We shall refer to this mode as **stimulated**, and allow the CLHA model to accept input within this mode. This leads us to the following choice of four modes for our CLHA model in order to cover the complete AP cycle: **stimulated (ST)**, **upstroke (UP)**, **early repolarization and plateau (EP)**, and **final repolarization and resting (FR)**.

As illustrated in Figure 10(b), where flows are momentarily ignored, the mode transition relation for $\mathcal{A}_1$ and $\mathcal{A}_2$ is generally cyclic in nature, although we allow the cell to return to mode **FR** from mode **ST** when it is under insufficient stimulus.

Due to its topology, $\mathcal{A}_1$ and $\mathcal{A}_2$ already possesses two common features of

excitable cells: **absolute refractoriness** and **graded response to sub-threshold stimulation**. Regarding the former, once a cell is excited, e.g., with a stimulus current, it enters an absolute refractory period, where the cell is nonresponsive to further excitation. This is reflected in our models by modes **UP** and **EP**, during which no further input is accepted and the cell cannot return to mode **UP**. Another excitation is possible only when the cell is in **FR**, and is captured with by a begin-stimulation event e_s that moves the model to mode **ST**.

Graded response to sub-threshold stimulation manifests in mode **ST**, where a cell accumulates its membrane voltage by accepting an input current. As soon as its voltage exceeds threshold V_T, the cell moves to mode **UP**. Otherwise, should the end-stimulation event $\bar{e}_s$ occur while $v < V_T$, the cell returns to mode **FR**. The cell returning to the resting phase is ultimately a consequence of the refractory modes: if the stimulus occurs at a sufficiently high pace, the second stimulation event may be missed.

The physiological separation of modes (or phases) of the AP has been our guiding principle for mode identification in our HA models. Recently, however, we have investigated the automated splitting of modes based on mathematical properties of AP waveforms other than their physiological meaning [32]. In the case of mode **ST**, there are two situations. In the single-cell case, since the outside stimulus can be specified before simulation begins, events e_s and $\bar{e}_s$ are well-defined. In spatial simulations, where a cell may also accept stimuli from its neighbors, events e_s and $\bar{e}_s$ represent respectively the abstraction of the process of the cell sensing its neighbors' potential and subsequently deciding to fire. Although the use of these events in the spatial setting may seem somehow arbitrary, spatial simulations using the HA models are both efficient and capable of reproducing reentry waves in cardiac tissues. HA-based spatial simulation is discussed in a separate paper [62].

3.1.2 Flows

The basic idea behind the flows of LTI-HA $\mathcal{A}_1$ is to capture the nonlinear dynamics (morphology) of a single AP in a piecewise-linear fashion. Since the AP (voltage v) is the only observed variable and we do not have other constraints on the dynamics of state variables, the flows in each mode can be described in a purely

linear manner as follows:

$$\dot{\mathbf{X}} = \mathbf{A}\mathbf{X} \tag{12}$$

$\dot{\mathbf{X}}$ is the first derivative of $\mathbf{X}$ with respect to time and $\mathbf{A}$ is a constant diagonal matrix. Thus, the only interdependencies among the state variables is through the observable v. Regarding the system's dimension, the greater the number of state variables, the greater its precision, with the complexity of the system description increased as well. We choose here to use three state variables, v_x, v_y, v_z, as a balance between precision and system complexity, with the overall membrane voltage v defined as follows:

$$v = v_x - v_y + v_z \tag{13}$$

Let $\mathbf{A} = diag(\alpha_x, \alpha_y, \alpha_z)$. The flows in modes **UP**, **EP** and **FR**, where no input is accepted, are given by:

$$\dot{v}_x = \alpha_x v_x, \quad \dot{v}_y = \alpha_y v_y, \quad \dot{v}_z = \alpha_z v_z \tag{14}$$

As discussed in detail in Section 3.3, curve-fitting techniques are used on a mode-by-mode basis to determine parameters α_x, α_y, and α_z such that $\mathcal{A}_1$'s output, i.e. the AP v, reproduces up to a prescribed error margin the AP of the original nonlinear system.

By considering a linear dependence on the input in mode **ST**, we still remain within the LTI-HA framework, but are now able to capture a family of trajectories, one per input:

$$\dot{v}_x = \alpha_x v_x + \beta_x I_s, \quad \dot{v}_y = \alpha_y v_y + \beta_y I_s, \quad \dot{v}_z = \alpha_z v_z + \beta_z I_s \tag{15}$$

As in the other modes, $\alpha_x, \alpha_y, \alpha_z$ and $\beta_x, \beta_y, \beta_z$ are the constants to be fitted.

3.1.3 Adaptability

The shape of the AP generated by $\mathcal{A}_1$ is fixed by the constant (matrix and scalar) parameters α, β, V_T, V_O and V_R. Moreover, the APD depends solely on the

stimulation frequency, as the time $\mathcal{A}_1$ spends in modes **ST**, **UP**, and **EP** (for fixed amplitude of I_s) is constant.

In contrast, the original nonlinear system has a phase space comprising infinitely many trajectories. To obtain an accurate approximation of this space, we derive CLHA $\mathcal{A}_2$ from $\mathcal{A}_1$ by generalizing $\mathcal{A}_1$'s constant parameters α, β, V_O and V_T to **cycle-constant** functions $\alpha(\theta)$, $\beta(\theta)$, $V_O(\theta)$ and $V_T(\theta)$, where θ is a normalized, one-cycle memory of the voltage. The derivation of $\mathcal{A}_2$ from $\mathcal{A}_1$ is based on the following observations:

- APs in different cycles share a similar morphology. It should thus be possible to to model them using equations possessing the same structure.
- According to the restitution property, AP morphology is principally determined by the length of the previous DI. This indicates that a control strategy based on a relatively simple, single-step memory unit will suffice for adaptability purposes.

CLHA memory. The DI in a given AP cycle influences the shape of the AP in the next cycle, in particular, the APD, stimulation voltage V_T, and overshoot voltage V_O. Regarding the APD, the time $\mathcal{A}_2$ spends in modes **ST** and **UP** is relatively small compared to the APD. One may therefore ignore the influence of the DI in these modes. The time $\mathcal{A}_2$ spends in modes **FR** and **EP**, however, can be considerable. For adaptability purposes, it therefore behooves us to make V_T, V_O and the time spent in modes **FR** and **EP** a function of the previous AP cycle's DI.

One can precisely model the DI by introducing a timer (a variable whose derivative with respect to time is 1) that is reset when $\mathcal{A}_2$ enters mode **FR** and measured when the stimulation event e_s occurs. To avoid the introduction of a new state variable into the model, we choose instead to linearly approximate the DI with the value of $\mathcal{A}_2$'s voltage v upon the occurrence of e_s. We remember this value by introducing a discrete variable v_n that is updated on the transition from **FR** to **ST** by the (assignment) action $v_n' = v$. (Note that v_n is "discrete" in the sense that its derivative is zero in all modes. This is in contrast to the term's traditional meaning: that of a variable whose range of possible values is discrete.)

Let $\theta = v_n/V_R$ and recall that the invariant of mode **FR** is $v \leq V_R$. We thus have that $0 \leq v_n \leq V_R$, and therefore $0 \leq \theta \leq 1$; i.e., θ is a normalized version of v_n. To see why it is a linear approximation of the DI, consider the triangles of Figure 11 having

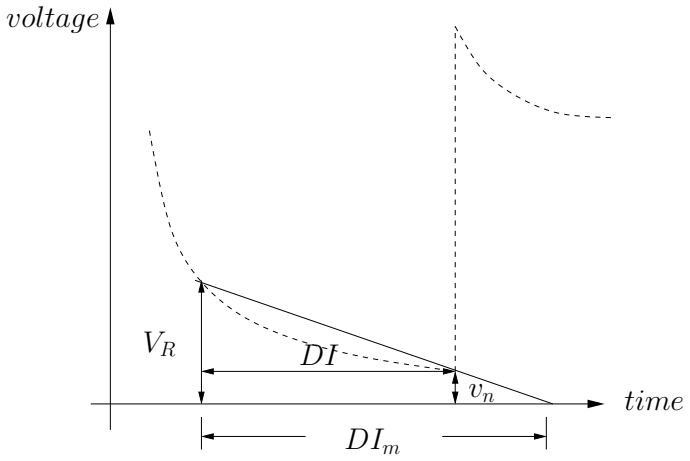

Figure 11: DI linearization.

bases DI and DI_m. Clearly they are similar triangles and therefore $(V_R - v_n)/V_R = DI/DI_m$. Since $\theta = v_n/V_R$, we have that $\theta = 1 - DI/DI_m$. One may thus conclude that θ is a (normalized) linear approximation of the DI of the previous AP cycle. (Technically speaking, θ is an *affine* approximation of the previous cycle's DI: a linear approximation followed by a translation.)

To make the parameter matrix α a function of θ in modes **FR** and **EP** of CLHA $\mathcal{A}_2$, we introduce the cycle-constant parameter matrix $\overline{\alpha}$ such that:

$$\overline{\alpha}_x(\theta) = \alpha_x \cdot f_x(\theta), \quad \overline{\alpha}_y(\theta) = \alpha_y \cdot f_y(\theta), \quad \overline{\alpha}_z(\theta) = \alpha_z \cdot f_z(\theta), \tag{16}$$

To refer to an α or f within a specific mode, we decorate them with superscript i, $0 \leq i \leq 3$, corresponding to modes **FR**, **ST**, **UP**, **EP**, respectively. The use of this convention can be seen, for example, in Table 1, where the definitions of functions f_x, f_y and f_z for modes **FR** ($i = 0$) and **EP** ($i = 3$) and different cell types (HH, LRd, NNR) are given. See also Figure 12, where a graphical depiction of $\mathcal{A}_2$ is given.

To see how θ influences the shape of the AP within modes **FR** and **EP**, first note that the AP is a monotonically decreasing function within these modes. Also note that f_x, f_y and f_z in these modes are functions of the form $1 + c\theta$, for some constant c. Then observe that the larger the value of θ, the larger the value of $f_x(\theta)$ (similarly for f_y and f_z), and therefore the larger the value of $\overline{\alpha}_x(\theta)$. Since $\overline{\alpha}_x(\theta)$

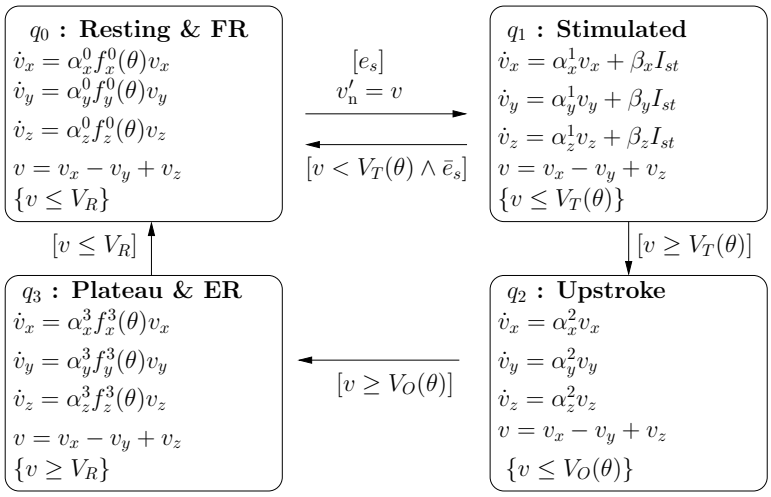

Figure 12: CLHA model of excitable cells.

appears as a coefficient of an exponential function in the analytical solution for v, a larger θ will make for a steeper (faster-decaying) AP in these modes, and therefore a shorter AP.

Further observe that, although θ is a linear approximation of the DI, its effect on the APD is *nonlinear*. This is because, in modes **FR** and **EP**, $\overline{\alpha}_x(\theta)$ appears as the exponent in one of the terms in the analytical solution for v (similarly for $\overline{\alpha}_y(\theta)$ and $\overline{\alpha}_z(\theta)$).

To model the dependency of the threshold voltage V_T and overshoot voltage V_O on the DI, we replace constants V_T and V_O with cycle-constant functions $V_T(\theta)$ and $V_O(\theta)$. Their definitions are also given in Table 1. Putting it all together, we obtain the CLHA $\mathcal{A}_2$ of Figure 12.

3.2 Formal Definition of the CLHA Model

Given an HA $\mathcal{A} = (X, G, \mathit{init}, \mathit{inv}, \mathit{flow}, \mathit{jump}, \mathit{event})$, we say that $\mathcal{A}$ is **cycle-linear** if the following conditions hold:

- The set of variables X is partitioned into a vector $\vec{x}$ of continuous variables and a vector $\vec{\theta}$ of discrete variables.

- There exists a simple cycle within the control-flow graph $G = (V,E)$ that includes all the vertices in V.
- θ is updated by all *jumps* to the initial mode.
- For a fixed θ and for each mode $v \in V$, $\mathit{flow}(v)$ is an LTI-system of the form $\dot{x} = \alpha(\theta)\,x + \beta(\theta)\,u$, where u is the input.
- For each mode $v \in V$, $\mathit{inv}(v)$ is a (linear) predicate of the form $x \# \gamma(\theta)$, where $\#$ is one of $\{\leq, \geq, <, >\}$ and $\vec{\gamma}(\theta)$ is a constant vector.
- For each switch $e \in E$, $\mathit{jump}(e).\mathit{guard}$ is a predicate having the same form as that of an invariant.

3.3 Fitting the CLHA Model to Excitable-Cell Models

In this section, we demonstrate the versatility of the CLHA model by fitting its parameters to successfully capture the AP morphology and restitution of three popular mathematical models of excitable cells: Hodgkin-Huxley (HH) [38], dynamic Luo-Rudy (LRd) [46], and neonatal rat (NNR).

Fitting the flow parameters of the CLHA excitable-cell model to a specific mathematical model involves the following two-step procedure: (1) Using a single representative AP, with θ set to 0, fit parameters α_w^i, β_w^i, $0 \leq i \leq 3$, $w \in \{x,y,z\}$. (2) Apply the well-known S1S2 protocol under varying frequencies to obtain a sequence of (DI,APD) pairs, which is then used to fit cycle-constant functions $f(\theta)_w^i$, $0 \leq i \leq 3$, $w \in \{x,y,z\}$, $V_O(\theta)$, and $V_T(\theta)$. Prior to executing step (2), we "guess" the form of these θ-related functions; the guiding principle here is to use elementary functions that take into account any extreme values these cycle-constant function may assume.

For example, consider $V_O(\theta)$ in the LRd model. In this case, V_O, the overshoot voltage, varies significantly from AP to AP, attaining a maximum value of 131.1 when $\theta = 0$, and a minimum value of 50.1 when $\theta = 1$. Choosing $V_O(\theta)$ to be the function $131.1 - 80.1\sqrt{(}\theta)$ ensures that V_O attains its proper maximum and minimum values over the range of APs used during the fitting process.

Curve fitting was performed using the unconstrained nonlinear optimization routines included in the MATLAB Optimization Toolbox [1]. At each time step,

	HH	**LRd**	**NNR**
$V_{\mathrm{T}}(\theta)$	26	44.5	39+9.7742θ
$V_{\mathrm{O}}(\theta)$	106.5	131.1-80.1$\sqrt{\theta}$	106.4-133.57θ^2
$V_{\mathrm{R}}(\theta)$	30	30	22+10.1091θ
$f_x^0(\theta)$	1	1	1+θ
$f_y^0(\theta)$	1	1	1+θ
$f_z^0(\theta)$	1	1	1+θ
$f_x^3(\theta)$	1	1	1
$f_y^3(\theta)$	1	$0.29e^{62.89\theta}+0.70e^{-10.99\theta}$	1+0.5798θ
$f_z^3(\theta)$	1	1	1

Table 1: Function definitions for CLHA $\mathcal{A}_2$.

target voltages derived via numerical integration of the HH, LRd, and NNR models are compared to the output from the CLHA model, also obtained via numerical integration. A time step of 0.005ms was chosen to ensure convergence of the implementation of the Euler method underlying the numerical-integration method. The goal of the optimization routines is to minimize the overall error, which is computed as the sum of the squares of the difference between the outputs of the CLHA model and the target voltages.

Although the optimization routines we used for curve fitting are completely automatic, the results they produce depend on the initial values supplied to them. In our case, we used a trial-and-error procedure to determine initial values that resulted in a satisfactory fit. The initial values we ultimately used are available upon request.

The functions and parameters we obtained using our fitting procedure are summarized in Tables 1 and 2.

For a single AP, a comparison of our CLHA model with HH, LRd and NNR is presented in Fig. 36. In the figure, solid lines represent the values obtained via numerical integration of the original nonlinear systems, while the dashed lines represent the values obtained via numerical integration of the corresponding CLHA automaton. Figure 14 compares the restitution functions of the CLHA and LRd models, when pacing the cell with different frequencies. It can be seen that we obtain a nonlinear dependence consistent with that observed for the nonlinear models,

	HH	LRd	NNR		HH	LRd	NNR
α_x^0	-0.1770	-0.0087	-0.0647	α_x^2	2.4323	-0.0069	0.3518
α_y^0	-10.7737	-0.1909	-0.0610	α_y^2	3.4556	0.0759	0.0395
α_z^0	-2.7502	-0.1904	-0.0118	α_z^2	2.8111	6.8265	0.0395
α_x^1	0.3399	-0.0236	-0.0473	α_x^3	-1.4569	-0.0332	-0.0087
α_y^1	4.5373	-0.0455	-0.0216	α_y^3	0.0339	0.0280	0.0236
α_z^1	0.0732	-0.0129	-0.0254	α_z^3	-0.9904	0.0020	0.0087
β_x	-3.6051	0.7772	0.7404	β_z	4.9217	0.2766	0.0592
β_y	0.0284	0.0589	0.0869				

Table 2: Parameter values for CLHA $\mathcal{A}_2$.

and also with that observed in live cells.

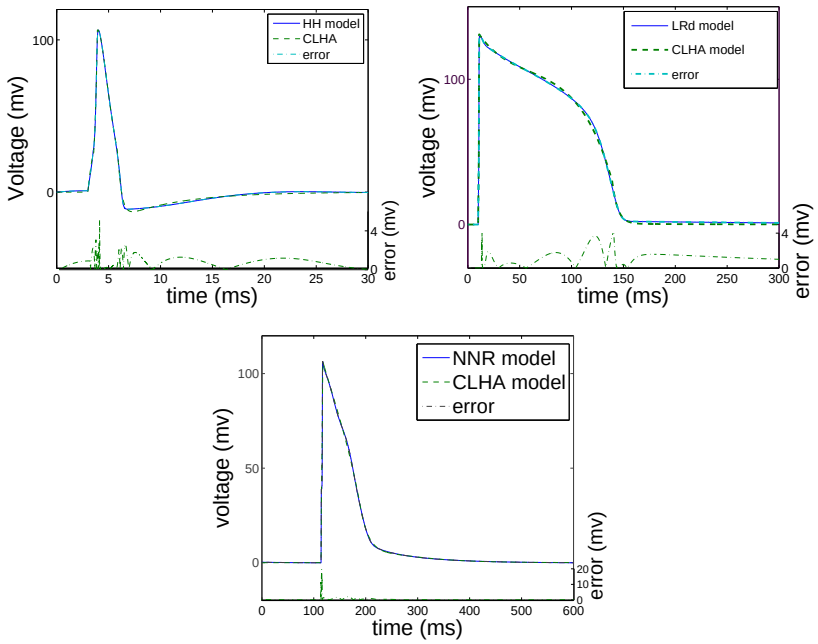

Figure 13: AP comparison of CLHA with: (a) HH (b) LRd (c) NNR

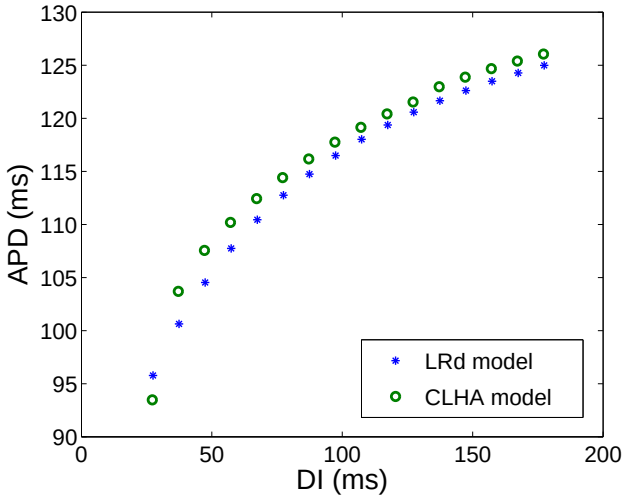

Figure 14: Restitution comparison with LRd.

3.4 Simulation of AP Propagation in Cardiac Tissues

To simulate cardiac-cell excitation propagation in homogeneous tissues, we need, in addition to a single-cell model, a diffusion model that describes the relationship of a cell with its neighbors. Here, we use a classic spatial 2D model as our diffusion model. The comparison of a single cell's solitary AP is demonstrated in Fig. 36(c).

We extended the simulations to model cell arrays as large as 400×400 cells. In these spatial simulations, the stimulation conditions (location and timing of the stimuli) were varied to simulate classical phenomena typical for cardiac tissue [30, 31, 51]. Running the original NNR model and the derived HA model under the same stimulation protocols, we observed similar spatiotemporal patterns, including spiral waves; see Fig. 15. This suggests that the proposed, reduced hybrid automaton not only captures the AP morphology for a single cell, but also correctly models the system in multicellular conditions when cell-to-cell communication in propagating the AP is critical. Thus, we show for the first time that Hybrid automata constitute a suitable framework for modeling multicellular excitable tissue. Additionally, a substantial improvement in computational efficiency was observed

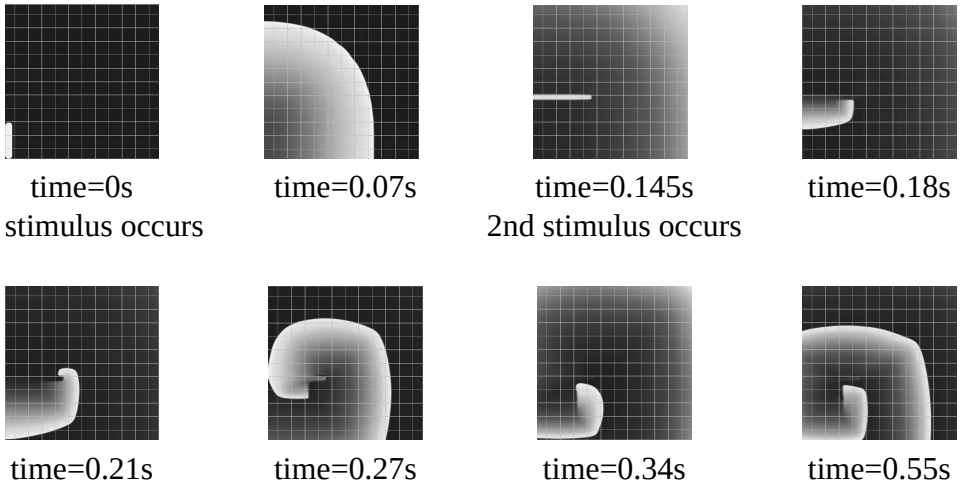

Figure 15: Snapshots during spatial simulation of excitation propagation in HA model.

with the HA model, as shown in Table 3. The benefit of the computational simplicity and scalability of the developed HA model will become especially valuable for large-scale 2D and 3D simulations with millions of cells.

cell array size	original(sec)	hybrid(sec)
2×2	5	3
4×4	9	3
8×8	26	6
16×16	93	14
32×32	365	51
64×64	1460	198
400×400	61833	8018

Table 3: Performance comparison for 2-second simulation.

3.5 Modeling Hyper-Polarization

In this work, hyper-polarization is referred to the behavior of a cardiac cell reacting to an external negative stimulation during **Plateau** mode. In this time period, a cell exhibits bifurcation behavior based on the amplitude of the input current

(Fig. 5). The goal is to catch the dynamics of Luo-Rudy model (LRd) in our CLHA model under the same input condition.

The previous CLHA model is not sufficient for the task because it abstracts the system as an *absolute refractory period* right after the **Upstroke (UP)** mode until **Final Repolarization and Resting (FR)** mode, which means the CLHA will not respond to further stimulations whether it is positive or negative. Hyper-polarization will not be incorporated without changing the CLHA structure and flow functions.

The construction of a new CLHA is consisted of the following two steps:

- Modify the transition graph according to the logic of hyper-polarziation.
- Fit the coefficients of the flow function based on the new data produced on the LRd model.

Basically, the above procedure is the same with the construction method of CLHA in Sec. 7.2, which shows that the CLHA model can be constructed accumulatively, one feature at a time. This evolution enables extendable design for complex systems.

3.5.1 CLHA Topology

Incorporation of hyper-polarization in the previous CLHA model assembles adding a decision branch in the original decision graph. We describe the decision process before and after the incorporation of hyper-polarization in a high level programming language style in Table 4 and Table 5.

Table. 4 shows the decision process of the CLHA derived using the method described in Sec. 7.2. The input is set to 0 in mode **EP** and **FR** because we suppose that cell in these two modes will be in the absolute refractory period and not response to further stimulation. To correctly model the hyper-polarization behavior, the cell have to response to negative input (outward currents) during **EP**. To accomplish this, we modify the code in mode **EP** in the following two ways:

- Add a statement to detect the existence of a negative input.
- A conditional statement on the strength of the stimulation that shows the two possibility of system behavior.

This part of codes is illustrated in Table 5. We introduce a new threshold value

```
 status = FR; // Initially, cell is in resting mode
 Vn = 0;
 vol = 0;
 while (true){
    input = checkInput();// check the existence of an input current
    update(status,vol,input,Vn); // update voltage according to the flow functions
    if (input>0){ // inward current
        status = ST; // switch to Stimulated mode
        //update membrane potential until the end of stimulation
        while(input > 0){
            update(status,vol,input,Vn);
            input = checkInput();
        }
        if(vol <= VT) { // Stimulation is not enough
            status = FR; //return to Resting mode.
        }
        else{ // threshold reached, fire an AP
            reset(Vn); //reset Vn and thresholds
            status = UP; // change status to Upstroke
            while(status == UP){
                update(status,vol,0,Vn,); // input = 0
                if( vol >= VO ){ // switch to Early Repolarization and Plateau
                    status = EP;
                }
            }
            while(status == EP){
                update(status,vol,0,Vn); // input = 0
                if( vol <= VR ){ // switch to Final Repolarization and Resting
                    status = FP;
                }
            }
        }
    }
} //while
```

Table 4: Decision process for a cardiac cell without hyper-polarization.

V_H which is the threshold between cell returning to **EP** and cell switches to **FR** at the end of a negative stimulation. We will show in the next subsection how to derive the value of V_H in detail.

3.5.2 Determining the Threshold and Flow Functions

The new threshold value V_H is the value determining the cell behavior at the end of a negative stimulation during Plateau phase. This value is not constant during the whole plateau phase according the the simulation results. It is monotonically increasing as the time distance between $S1$ and $S2$ stimulations, which is illustrated in Fig. 16. The solid lines show the cases where cell returns to EP and dashed lines show the cases then cell switches to FR.

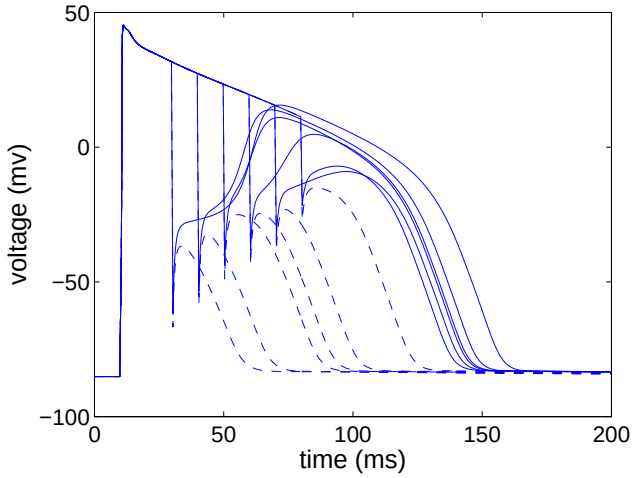

Figure 16: Bifurcation behavior of LRd model.

As there is no global time variable in the CLHA model, in the same spirit of Sec. 7.2, we use the memory unit v_n to "remember" the voltage at which $s2$ happens, and use a function of v_n to define V_H. Actually, we can approximate V_H in a linear function $V_H = f_{V_H}(v_n)$, as can be seen in Fig. 17.

The cell behavior after a negative input is determined by two factors: *when* is the negative input and *how strong* is the input. The timing factor is captured by memory unit v_n, and the strength of the current determines *how deep down* the voltage can reach at the end of the stimulation. As these two factors are orthogonal

```
status = FR; // Initially, cell is in resting mode
Vn = 0;
vol = 0;
while (true){
   input = checkInput();// check the existence of an input current
   update(status,vol,input,Vn); // update voltage according to the flow functions
   if (input>0){ // inward current
       status = ST; // switch to Stimulated mode
       //update membrane potential until the end of stimulation
       while(input > 0){
           update(status,vol,input,Vn);
           input = checkInput();
       }
       if(vol <= VT) { // Stimulation is not enough
           status = FR; //return to Resting mode.
       }
       else{ // threshold reached, fire an AP
           reset(Vn); //reset Vn and thresholds
           status = UP; // change status to Upstroke
           while(status == UP){
               update(status,vol,0,Vn,); // input = 0
               if( vol >= VO ){ // switch to Early Repolarization and Plateau
                   status = EP;
               }
           }

           while(status == EP){
               input = checkInput();
               if (input == 0){
                   update(status,vol,0,Vn); // input = 0
                   if( vol <= VR ){ // switch to Final Repolarization and Resting
                       status = FR;
                   }
               }
               elseif (input < 0){ //negative input currents
                   update(Vn); // update Vn and VH
                   while (input < 0){
                       update(status,vol,input,Vn);
                   }
                   update(Ve); //Ve is the voltage at the end of stimulation
                   if(vol<VH){ // cell switches to Resting mode
                       status = FR;
                   }
                   else{ } //remaining in EP mode
               }
           }}}}}
```

Table 5: Decision process for a cardiac cell with hyper-polarization.

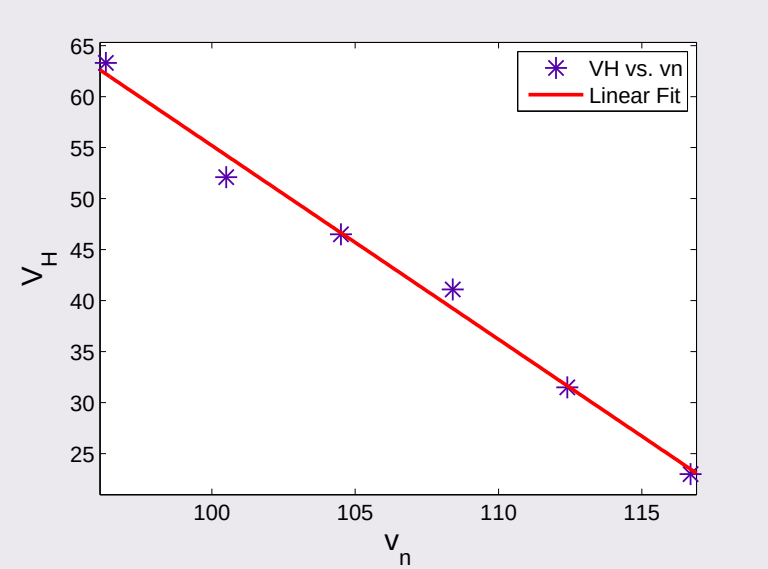

Figure 17: Linear dependence of V_H on v_n

to each other, we have to introduce another memory unit v_e to record the membrane potential at the end of $s2$ stimulation and now the flow function is also a function of v_e.

The result is illustrated in Fig. 18. We put the simulation results from LRd and the CLHA model side by side for a better comparison. Each row gives the superposition of multiple simulation runs of each model for a given timing of $S2$ and the range of the input currents (I_{st}), as shown in the title of each sub-figure.

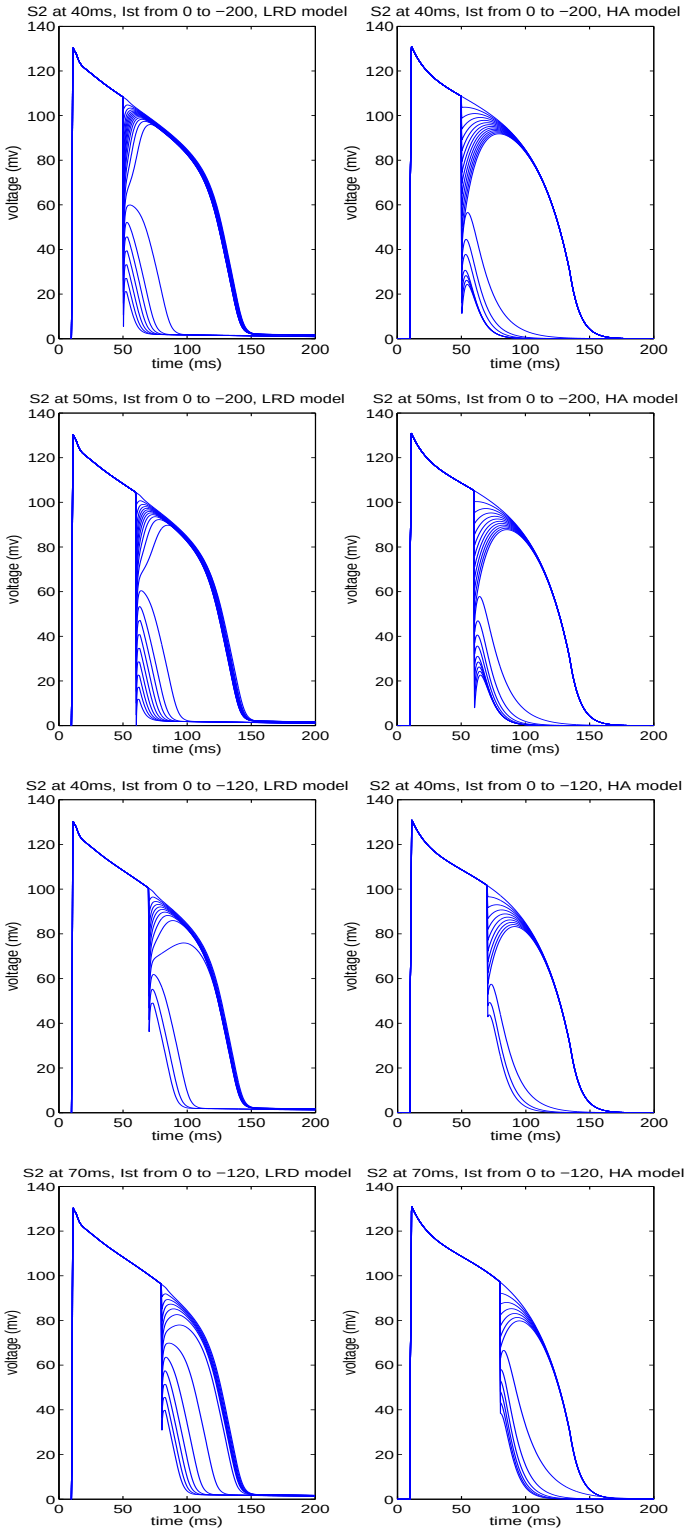

Figure 18: Comparison of the simulation result from LRd model and CLHA model.

Chapter 4

Learning Cycle-Linear Hybrid Automata

In previous chapters, we showed that it is possible to construct a conceptually simpler HA model for ECs that approximates with reasonable accuracy their electrical properties. We called these HA *Cycle-Linear HA* (CLHA) to highlight their cyclic structure and the fact that, while in each cycle they exhibit linear dynamics, the coefficients of the corresponding linear equations and mode-transition guards may vary in interesting ways from cycle to cycle.

The manual construction of CLHA, however, proved to be a tedious task, and the CLHA so derived were tied to a particular type of EC and to a particular species. Moreover, since recent advances in measuring *in vitro* the electrical activity of ECs have resulted in the availability of extensive data sets, it was natural to turn our attention to the following question: *Given a training set of electrical measurements of an EC, is it possible to automatically learn a CLHA that approximates the behavior of the EC up to a required error margin?*

In this chapter we address this question, by presenting a methodology for automatically learning CLHA models for two types of ECs: the squid giant axon and the guinea pig ventricular cell. To the best of our knowledge, these are the most accurate approximation models (with per-AP-cycle linear dynamics), developed for these ECs to date, both in terms of electrical-signal morphology and typical excitable-cell characteristics such as refractoriness and restitution.

To simplify the process of obtaining training sets, we used *virtual* measurements obtained by applying the so-called *S1S2*-protocol to existing nonlinear models of these ECs. Extending the method outlined here to *in vitro* data obtained in the laboratory of the fourth author is a direction for future work.

The learning technique we have developed for CLHA is also of independent interest, as we learn all aspects of excitable-cell CLHA models up to a given error margin, including the number of modes; for each mode, the dimension of the state space and the coefficients of its linear time-invariant dynamics; and all aspects of the mode switching logic, including the jump conditions, thresholds and resets. To do so, we use the modified Prony's method to obtain an exponential fit for the continuous per-mode linear dynamics. Moreover, in learning the CLHA, we make no *a priori* assumptions about the dimension of the state space of the nonlinear system we are targeting, nor the degree of its input and output.

We also learn the functions that adjust a CLHA's mode dynamics and switching logic on a per-cycle basis. This aspect of our technique is critical in the case of excitable cells, which exhibit the following *restitution property*: the longer the recovery time for an EC, the longer in duration its subsequent *action potential*.

4.1 Learning Method

Given a training set of APs generated by applying the *S1S2*-protocol to an excitable cell of a particular species, our methodology for learning the CLHA that approximates the cell's behavior up to a given error margin consists of two phases. In the first phase, we obtain for each AP a linear Hybrid automaton (LHA) whose output is within the specified error bound. This involves identifying the segments of the APs that correspond to the modes of the LHA, deriving the flows for each mode, and the guards and reset maps for each transition. In each mode, we use the modified Prony's method (MPM) [52] to approximate the AP with a (normalized) linear dynamics, i.e., with a sum of exponentials.

In the second phase, we derive a CLHA that combines the behavior of all the LHAs and therefore captures all the APs in the training set. We exploit the fact that the coefficients defining the flows, guards, and reset maps of the CLHA are functions of the *epoch* variable which is updated during an *epoch transition*. We choose

the variable to be a voltage-valued variable called v_0 and epoch transitions to be those that are brought about by the occurrence of a stimulus. In finding the snapshot map which sets the value of the epoch variable in the post-state of epoch transitions, we once again use MPM. Specifically, we estimate the voltage-dependent coefficients of the CLHA as an exponential regression of the constant coefficients in the LHAs obtained in the first phase.

Assumptions. Our goal is to derive a CLHA, the output of which is within $\pm 2mv$ of the output of the Luo-Rudy model, under the following class of stimuli: each stimulation is a step of amplitude $-80\ \mu\mathrm{A}/\mathrm{cm}^2$, duration $0.6ms$, and BCL between 160 and $400ms$. The set of 25 APs sampled every $0.2ms$, corresponding to BCL 160 to $400ms$, in $10ms$ intervals, serves as the *training set* for deriving the CLHA. The performance of the learned CLHA is evaluated on the *test set* consisting of APs with BCL from 165 to $405ms$, in $10ms$ intervals, sampled at the same frequency.

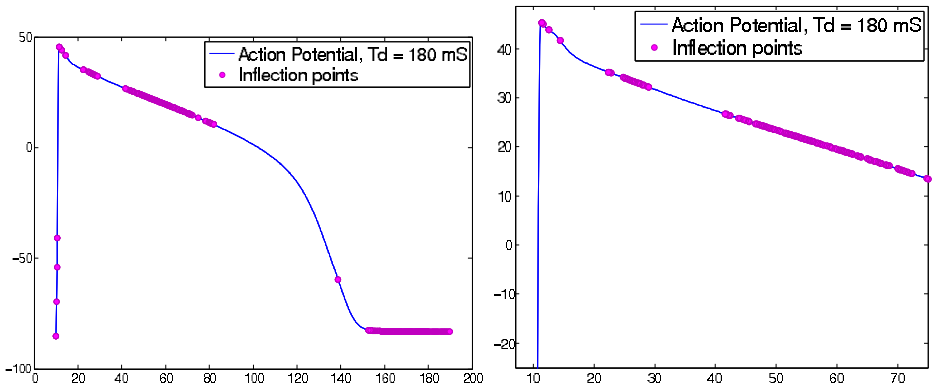

Figure 19: Null/inflection points in the LRd APs.

Identifying Modes. To discover the points in the APs that correspond to mode transitions in the target LHAs, we computed the null points (zeros of the first-order derivative) and the inflection points (zeros of the second-order derivatives) of the APs. This approach worked very well for the HH model, and the sections of APs between successive null or inflection points were identified as the modes of the LHAs.

When directly applied to the LRd model, this approach yielded far too many modes. In particular, there exist trains of inflection points in the **P** and **R** phases of the APs (see Figure 19). This was somewhat surprising because the AP of these phases appears as rather smooth line segments corresponding to "stretched" inflection points. The higher-order nonlinearity of the LRd model seems to have dealt with such segments by generating trains of points whose tangent (first-order derivative) difference was smaller (in absolute value) than 10^{-5}. Based on this observation, we designed our own parameterized filter to eliminate such long sequences of closely-spaced inflexion points. The filter parameter enable us to increase or decrease the number of segments and thereby achieve the desired accuracy of the CLHA.

Using the MPM described below, we were able to approximate each segment with two exponentials and the entire AP to within the desired accuracy. Since, however, this approach seemed to split each of the **E** and **F** phases in two, we decided to eliminate one inflection point in each. In doing so, we were not able to maintain the desired accuracy, unless we moved down the end-point of phase **P** and up the starting-point of phase **R**. The correctness of both transformations was confirmed by analyzing higher-resolution APs, where these points were indeed very close to their inferred position. The final seven points chosen are shown in Figure 20(a).

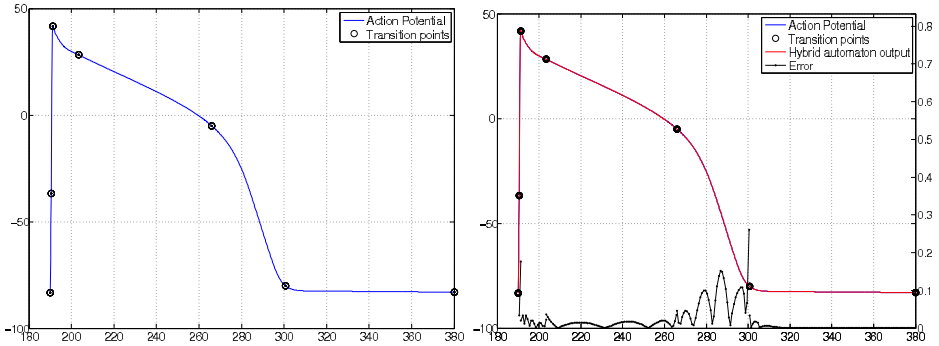

Figure 20: (a) Inflection points after filtering. (b) Hybrid-automaton output.

Using Modified Prony's Method to Obtain LHA. The null/inflection points partition the AP into sections defining six modes of the LHA: **S**, **U**, **E**, **P**, **F** and **R**. We

denote the set of modes by $\wp$. Since these modes are always visited in order, the voltages of the six inflection points define the guards (thresholds) for the corresponding transition edges. We denote the transition voltages by V_p, where $p \in \mp$, is the mode in the post-state of the transition. For example, in the AP of Figure 20(a), the transition from **U** to **E** occurs at $V_{\mathbf{E}} = 45.32mv$. To completely define the LHA, it remains to define the flows and the reset maps; for this we use the modified Prony's method [52].

The modified Prony's method is a technique for fitting exponential or sinusoidal functions to time-series data. For fixed n, MPM minimizes the $L2$ distance between time-series data and any function y that solves a differential equation with constant coefficients:

$$\sum_{i=1}^{n+1} c_i \frac{d^{i-1}y}{dt^i} = 0. \tag{17}$$

Depending on the coefficients c_i, the function estimating the solution of Equation 17 may be a complex or a real exponential, damped or undamped sinusoids. Furthermore, the input to the algorithm can be noisy periodic samples from the actual solution. Because of these attractive features, MPM has found many practical applications.

Suppose the voltage in mode $p \in \mp$ of the AP can be approximated as a sum of exponential functions:

$$v(t) = \sum_{i=1}^{n} a_{ip} e^{b_{ip}t} \tag{18}$$

Then, we can specify the flows in each mode as :

$$\begin{aligned} \forall\, i \in \{1,\ldots,n\},\ \dot{x}_i &= b_{ip}x_i \text{ and } x_i(0) = a_{ip} \\ v &= \sum_{i=1}^{n} x_i, \end{aligned} \tag{19}$$

where the x_i's are the state variables. The initial condition on the state variables is set by the reset map of the transition from the previous mode. The accuracy of the above approximation is a function of n, that is, the number of state variables used. Using the MPM with $n = 2$, we obtained, approximations that were within the acceptable error bounds for all modes.

The output of the resulting LHA, the original AP, and the error between the two, are plotted in Figure 20(b). We apply this procedure to obtain an LHA for each AP in the training set. The output of these automata, superimposed on the original APs, are shown in Figure 21(a).

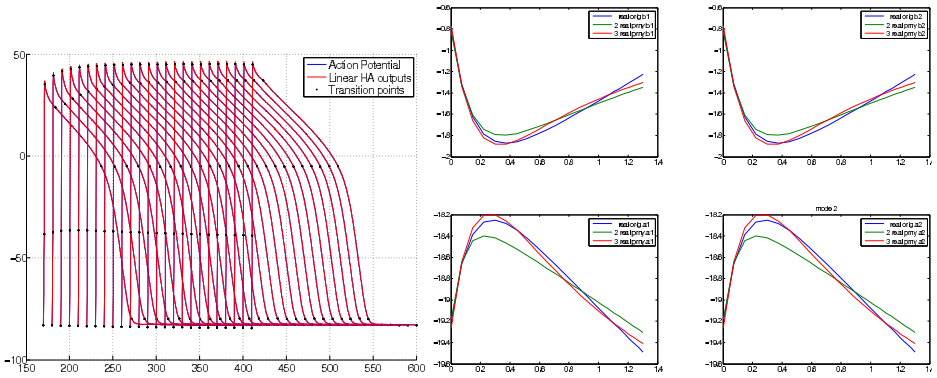

Figure 21: (a) Original APs and superposed LHA outputs for training set. (b) Sums of 2 and 3 exponentials for estimating a_1, a_2, b_1 and b_2 for mode **U**.

Linear to Cycle-Linear HA. From the first phase, we obtain for each AP in the training set and for each mode $p \in \mp$, the transition voltage V_p for the guards, and the coefficients b_{1p}, b_{2p}, and a_{1p}, a_{2p} corresponding to the the differential equations and initial values for the state variables x_1 and x_2. In other words, we obtain one linear hybrid automaton approximating each of the APs in the training set.

In the second phase, we combine these LHAs into a single CLHA by using the transition to mode **S** (stimulus arrival) as the epoch transition, setting the value of the epoch variable v_0. We call the value of v_0 the *epoch voltage*. For each mode, we find a function mapping v_0 of each LHA to transition voltages and coefficients; this function implicitly defines the snapshot map. We once again use sums of two exponentials for these functions and obtain their coefficients by applying MPM. These functions are defined below, where $p \in \mp$ and $i \in [1..2]$:

$$\begin{aligned} V_p(v_0) &= \vartheta_p \quad e^{\theta_p v_0} + \vartheta'_p \quad e^{\theta'_p v_0} \\ a_{ip}(v_0) &= \alpha_{ip} \quad e^{\lambda_{ip} v_0} + \alpha'_{ip} \quad e^{\lambda'_{ip} v_0} \\ b_{ip}(v_0) &= \beta_{ip} \quad e^{\gamma_{ip} v_0} + \beta'_{ip} \quad e^{\gamma'_{ip} v_0} \end{aligned}$$

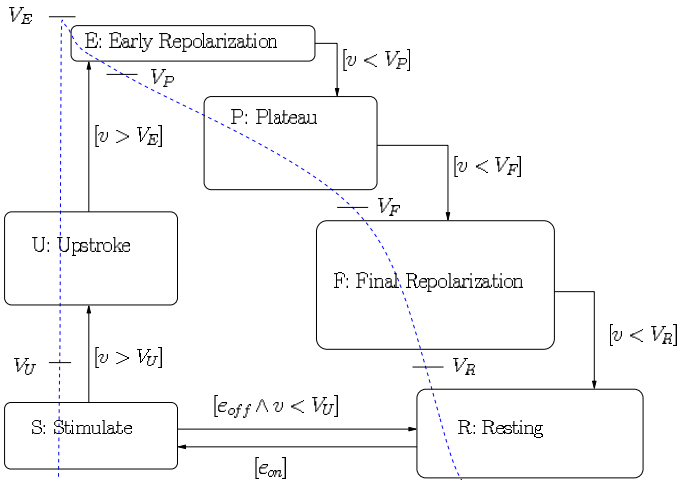

Figure 22: Structure of the CLHA.

Thus, a_{ip}, b_{ip} and V_p in the CLHA depend on the AP value stored in variable v_0 on the epoch transition between modes **R** and **S**. The way MPM approximates a_{1U}, a_{2U}, b_{1U} and b_{2U} with sums of two or three exponentials is shown in Figure 21(b). The structure of the CLHA thus obtained is given in Figure 22. For simplicity, the figure does not show the actions on the transitions and the flows within the modes.

While the above equations give the general pattern for the transition voltages and coefficients, a few observations are in place. First, by construction, V_F and V_R are constant in all LHAs and therefore no exponential fitting is necessary for the CLHA. Secondly, the a_i and b_i coefficients of modes **F** and **R** are up to a very small variation the same in all LHAs. Although we expressed them as functions in the CLHA, we are confident that using constants instead would have still satisfied the required accuracy. Thirdly, for the rest of the modes, the a_i and b_i obtained for the LHAs are complex values. We therefore separately fitted their real and imaginary parts. The constant coefficients ϑ_p, ϑ'_p, θ_p, θ'_p, α_{ip}, α'_{ip}, λ_{ip}, λ'_{ip}, β_{ip}, β'_{ip}, γ_{ip} and γ'_{ip} are complex too. Finally, due to space restrictions, we defer including a table with all voltage and coefficient values to the full version of the paper.

4.2 Simulation results

We have implemented the above-described learning technique in MATLAB, and applied it to both the HH and LRd models. The accuracy of the resulting CLHA was analyzed on both the training and test sets. Due to space constraints, the results on the simpler HH model are omitted.

The output of the CLHA on the LRd test set is shown superposed on the original APs in Figure 43(a). As can be observed, the morphology of the output, as well as the required accuracy, is maintained on this set.

In Figure 43(b), the restitution curve obtained from the CLHA by running it on the v_0's specified in the test set is compared to the restitution curve obtained from the APs in the test set. Although not perfect, the results are very satisfactory. To our knowledge, these are the best results among the LRd-approximation models proposed so far.

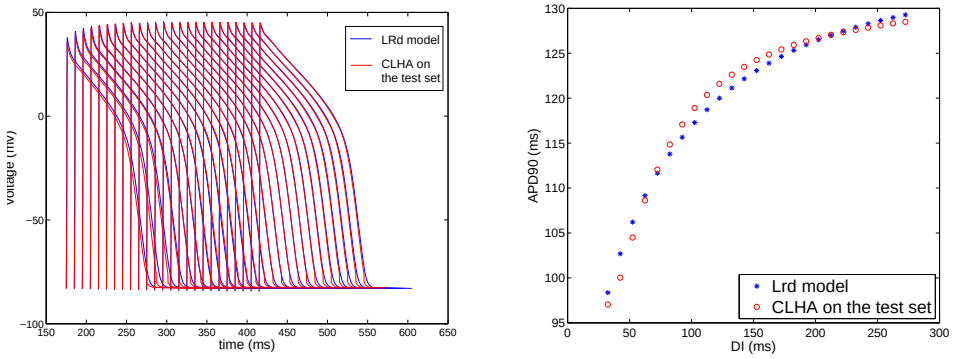

Figure 23: (a) Comparison of AP. (b) Comparison of restitution curve.

4.3 Discussion

We have developed a learning/identification technique for cycle-linear hybrid automata (CLHA), and applied it to a classical, highly nonlinear model of ventricular cardiac myocytes. The technique of hybrid-automaton identification has been previously used in a number of communication and control applications, including interplanetary life-support systems [33], dynamic power management [24],

autonomous systems and intelligent robots [28, 40], and figure tracking [53]. To the best of our knowledge, our application of this technique in the area of systems biology, in general, and excitable cells, in particular, is the first of its kind.

Our approach to hybrid-automaton identification is further distinguished from prior work in the area by the novelty of the identification technique itself. Specific contributions in this regard include the following: (1) Our approach is applicable to continuous-time nonlinear systems that exhibit some level of periodicity and adaptation. Given such a system, the CLHA we learn are also continuous-time, specifically, linear time-invariant (LTI). In contrast, the techniques of [13, 61] target discrete-time PWARX (piecewise-affine auto-regressive exogenous) models. Furthermore, in contrast to these approaches, when learning the CLHA for a system S, we make no *a priori* assumptions about the dimension of S's state space nor the degree of its input and output.

(2) Our technique learns all aspects of a hybrid automaton, including the number of modes; for each mode, the dimension of the state space and the coefficients of its LTI dynamics; and all aspects of the mode switching logic, including the jump conditions, thresholds and resets. To do so, we use a modified Prony method to obtain an exponential fit for the continuous per-mode linear dynamics. Cf. [61], where polynomial fitting is used for the case of discrete-time PWARX systems.

(3) We also learn the functions that adjust a CLHA's mode dynamics and switching logic on a per-cycle basis. This aspect of our technique is critical in the case of excitable cells because of their *restitutional* nature (see Section 1.2). In this case, the coefficients of the mode dynamics and the voltage thresholds are functions of V_0, the cell's initial transmembrane voltage for the current cycle.

Chapter 5

Symbolic Analysis of the Neuron Action Potential

In this chapter, we present a simplified HA model which can be passed to a reachability analysis tool d/dt to verify formal properties of neurons. The property we are interested is called the bifurcation behavior of neurons subject to external stimuli with different strength and duration. The formal analysis is important as the system dynamics are usually infinite with infinite possible inputs or parameters. Before the reachability analysis technique, the only method is through simulations, which is not complete. The goal of this study is that we want to prove that neurons' behavior for a set of inputs (infinite many) can be determined with a single run of reachability analysis algorithm, which is attractive and efficient for studying neuron's reaction under complex situations.

We first introduce this tool then presents the analysis and result from reachability study of HA model.

5.1 Introduction to the Reachability Analysis Tool d/dt

The d/dt tool performs forward reachability analysis on LHA, presenting the final result in a graphical form. It uses convex polyhedral packages for this purpose, representing reachable sets of states as unions of convex polyhedra. In order for d/dt

to perform reachable-set computations, one has to provide it with the following data:

- *Dimension*: The number of the variables in the input LHA.
- *Initloc*: The initial mode of the LHA.
- *Initset*: The initial-range polyhedron of the state variables.
- *Badset*: The unwanted polyhedron area, in the case of safety analysis.
- *Locations*: The modes of the LHA.
- *Matrix A* and *scale B*: Matrix and scale as in Definition 1.1.1.
- *Inputset*: A polyhedron bounding the range of U for each mode.
- *Transitions*: The guard polyhedron and target mode for each switch.
- *Stayset*: The invariant polyhedron for each mode.
- *Limits*: The range polyhedron on which reachability analysis is performed.

Depending on the system to be analyzed, some of the above specifications may be optional. The users can also provide their own computation parameters (like the integration step) in a separate file to control the balance of computation time and precision. If there no such file is provided, default values are used.

5.2 Bifurcation Analysis of the All-Or-Nothing Response of Neurons

In the previous chapters, we have developed a series of CLHA for ECs. The CLHA so derived is able to capture important EC properties—including the AP morphology up to a prescribed error margin and the nonlinear restitution property—despite having having only two (or three) continuous state variables.

For the purpose of bifurcation analysis, we will restrict our attention to the derivation of a simple neuronal LHA. We will then input this LHA to d/dt in order to symbolically analyze its response to any possible input over an arbitrary time domain within a given time interval.

Learning the Neuronal LHA. As in [32, 62], the automatic learning method we use for neuronal LHA proceeds in two stages:

- Identify the topology of the LHA, i.e. the design of its control graph.
- Identify for each control-graph mode, the dynamics of the LHA model.

The choice of modes is based on the observation that the AP for different cell types (neuron, cardiac myocyte, etc.) or different species (guinea pig, neonatal rat, etc.) may exhibit different waveforms, but they all possess the following two phases within a cycle: a `Rising` phase and a `Falling` phase; see Figure 24. For the purpose of mode identification, we also need to identify the time period during which the cell is subject to external stimulation. We shall refer to this mode as `Stimulated`, and allow the LHA model to accept input within this mode. This leads to the splitting of the rising phase into modes `Stimulated` and `Rising`.

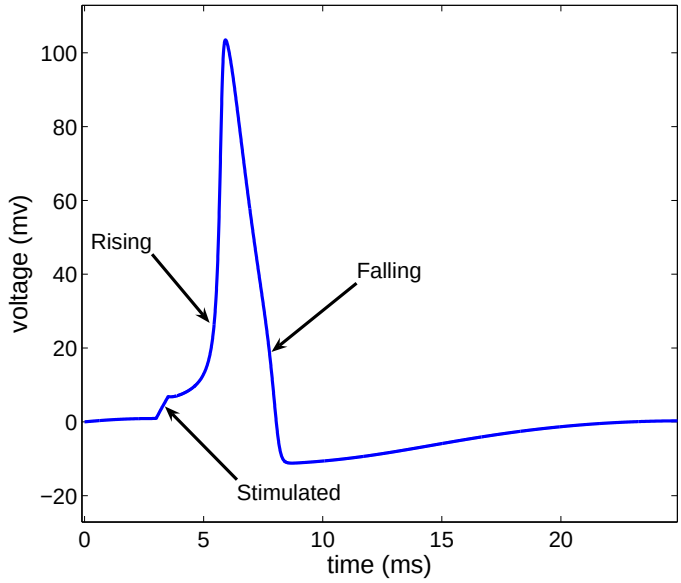

Figure 24: Rising and falling phase of neuron.

In a first version of the automaton, we use a begin-stimulus event e_s and an end-stimulus event $\bar{e}_s$ to effect this separation. When external stimulation begins, i.e., upon the occurrence of e_s, the LHA switches to mode `Stimulated`, in which the cell accumulates its membrane voltage by accepting an input current. If upon termination of the stimulation, i.e., upon the occurrence of the event $\bar{e}_s$, the magnitude of the received stimulation is sufficiently strong, the cell fires an AP by switching to

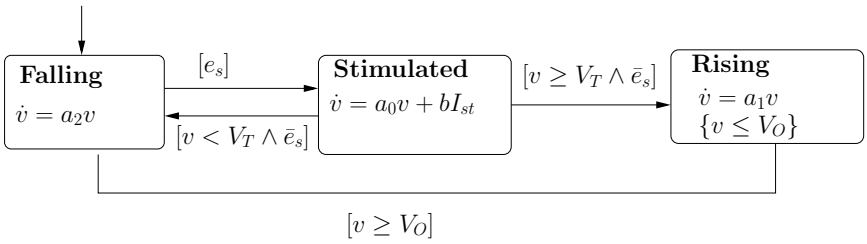

Figure 25: Graphical representation of neuronal LHA.

mode `Rising`; otherwise it returns to mode `Falling`. In the former case, the LHA will switch from mode `Rising` to `Falling` when it passes the maximum voltage point.

Since the voltage is the only observable in which we are interested and since bifurcation, the phenomenon of interest, only occurs at the end of stimulation, we tolerate a larger error margin within mode `Falling`. As a consequence, our learning algorithm is able to derive an acceptable LHA with only one continuous state variable representing the AP. Certainly, this might be not the case for other observables. The LHA so derived is depicted in Figure 25.

The flow function is of the form $\dot{v} = a_0 v + bI_{\text{st}}$ for mode `Stimulated` and $\dot{v} = a_i v$ $(i = 1,2)$ for the other two modes (these modes are therefore called refractory modes). The threshold values V_{O} and V_{T} are constants determined by analyzing the data produced by the HH model. The coefficients a_i for $i = 0,1,2$, and b are also automatically learned by analyzing the data produced by the HH model via numerical integration. Their precise values are given in the Appendix.

Encoding the LHA in d/dt. In order to study the behavior of the neuronal LHA subject to input stimuli of various shapes, intensities and duration, one has to manipulate two parameters: the value of $\texttt{I}_{\texttt{st}}$ and the interval between the begin- and end-stimulus events. The manipulation of the first parameter can be easily accomplished in d/dt by using the polyhedron $\texttt{0} \leq \texttt{I}_{\texttt{st}} \leq \texttt{11}$, where 0 is the minimum and 11 is the maximum value for $\texttt{I}_{\texttt{st}}$.

The manipulation of the second parameter, however, is more involved. For this purpose, we introduce an explicit clock variable `x`, whose derivative is allowed to vary within the polyhedron $\texttt{1} \leq \texttt{dx/dt} \leq \texttt{1.4}$. The lower bound of 1 is a natural one for a skew-less clock, while the upper bound of 1.4 encoded the range of stimulus duration we were interested in investigating. That is, it is easily observed that the

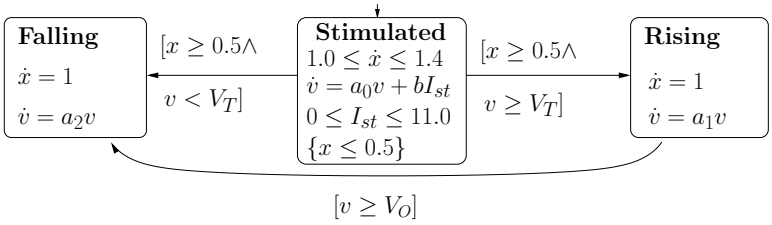

Figure 26: Graphical representation of LHA input to d/dt.

larger the derivative, the faster clock. As such, for an input stimulus of duration say `0.5`, although in the LHA we compare `x` to this constant value, the larger the value of the derivative, the smaller the amount of time that actually passes before this timer expires.

The flow functions we thus obtain for the LHA we input to d/dt are given in Equation 20.

$$\begin{bmatrix} \dot{x} \\ \dot{v} \end{bmatrix} = \begin{bmatrix} 0 & 0 \\ 0 & a_0 \end{bmatrix} \begin{bmatrix} x \\ v \end{bmatrix} + \begin{bmatrix} i_1 \\ i_2 \end{bmatrix} \qquad \begin{bmatrix} \dot{x} \\ \dot{v} \end{bmatrix} = \begin{bmatrix} 0 & 0 \\ 0 & \alpha^i \end{bmatrix} \begin{bmatrix} x \\ v \end{bmatrix} + \begin{bmatrix} 1 \\ 0 \end{bmatrix} \quad (20)$$

The constraints we place on the intensity and duration of $\mathtt{I_{st}}$ are encoded in mode `Stimulated` by requiring that $\mathtt{1} \leq i_1 \leq \mathtt{1.4}$ and $\mathtt{0} \leq i_2 \leq \mathtt{11}$, respectively. Also, to ensure a baseline timeout period of `0.5` for `x`, the invariant $\mathtt{x} \leq \mathtt{0.5}$ is added to mode `Stimulated` and the guard condition $\mathtt{0.5} \leq \mathtt{x}$ is added to the transitions emanating from this mode. The resulting automaton is depicted in Figure 26. Its full description in d/dt is given in the Appendix.

It can be seen that the automaton (with explicit time) of Figure 26 is equivalent to the parallel composition of the automaton (where time is implicit) of Figure 25 with an environment automaton, providing an input stimulus of various form and duration, delineated by begin- and end-stimulus events, respectively.

Analysis Result Let us henceforth refer to the neuronal LHA of Figure 25 (where time is implicit) as LHA1, and the neuronal LHA of Figure 26 (the one input to d/dt, where time is explicit) as LHA2. In this section, we first compare the simulation results for a single AP, resulting from a rectangular-pulse stimulus, using the LHA1 and HH models. We then present the results of our symbolic reachability analysis

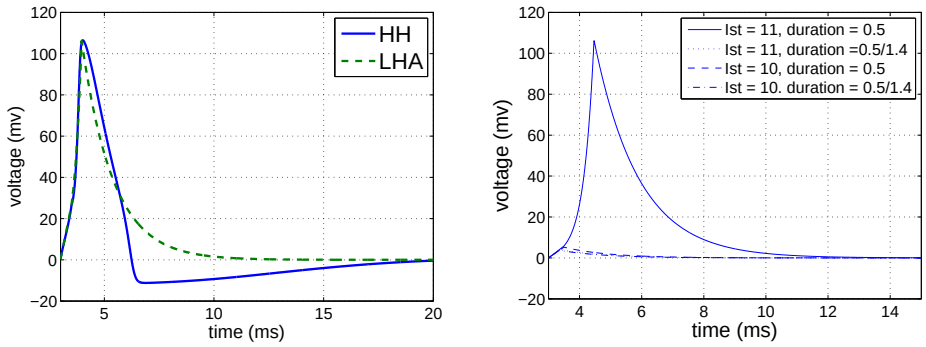

Figure 27: (a) AP comparison: LHA1 vs. HH. (b) Bifurcation in LHA1

for LHA2, where all input stimuli (of any form and duration within given intervals) are automatically (symbolically) taken into account by d/dt. Our results, given in terms of LHA2's reachable state sets, clearly demonstrate the bifurcation property over this infinite input set.

Figure 27(a) compares the simulation of a single AP using the LHA1 and HH models The initial condition for the voltage was the same in both models. The parameter values considered for the HH model were as follows: $\bar{g}_{\mathrm{Na}} = 120\mathrm{mOhms}^{-}1/\mathrm{cm}^2$, $\bar{g}_{\mathrm{K}} = 36\mathrm{mOhms}^{-}1/\mathrm{cm}^2$, $\bar{g}_{\mathrm{L}} = 0.3\mathrm{mOhms}^{-}1/\mathrm{cm}^2$, $E_{\mathrm{Na}} = 55.0\mathrm{mv}$, $E_{\mathrm{K}} = -72.0\mathrm{mv}$, $E_{\mathrm{L}} = -50.0\mathrm{mv}$, $C = 1$. The stimulation current for both models was a rectangular pulse with an amplitude of $50\mathrm{uA}/\mathrm{cm}^2$ and a duration of 0.5ms. As can be observed, the AP is better matched during the rising phase than in the falling phase, as our focus with the neuronal LHA model is on whether or not an AP will be fired under different input currents. The undershoot during the falling phase is missed in the LHA1 model, a compromise made in favor of the model's simplicity.

The bifurcation seen in Figure 27(b) occurs when the stimulation current increases from $10\mathrm{uA}/\mathrm{cm}^2$ to $11\mathrm{uA}/\mathrm{cm}^2$. When the current reaches $11\mathrm{uA}/\mathrm{cm}^2$, an AP is fired, while for a current of $10\mathrm{uA}/\mathrm{cm}^2$, only a small bump is observed.

We conducted two sets of reachability analysis on the LHA model: one with the input current ranging within interval $[0, 10]\mathrm{uA}/\mathrm{cm}^2$ and the other with the input current ranging within interval $[0, 11]\mathrm{uA}/\mathrm{cm}^2$. The output of d/dt's reachability algorithm is a rendering of the shape of the reachable set in each mode. For a two-dimensional system such as LHA2, the reachable set is planar.

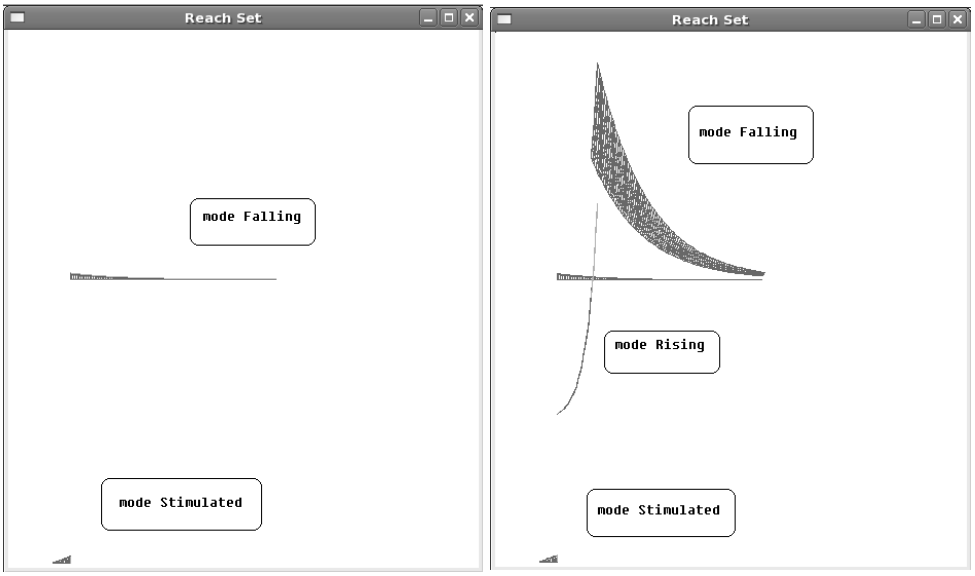

Figure 28: (a) Reachable set for $I_{st} \in [0, 10]$. (b) Reachable set for $I_{st} \in [0, 11]$.

Figure 28(a) shows the reachable set for a stimulus current between $0\text{uA}/\text{cm}^2$ and $10\text{uA}/\text{cm}^2$. Only modes `Falling` and `Stimulated` are reached during the computation. Figure 28(b) shows the reachable set for a stimulation current between $0\text{uA}/\text{cm}^2$ and $11\text{uA}/\text{cm}^2$. In this case, we see that all three modes are reached. In particular, bifurcation is observed in mode `Falling`: the reachable set for this mode is composed of an upper part, reached by switching from mode `Rising`, when an AP occurs, and a lower part, reached by returning from mode `Stimulated`, when an AP fails to occur.

Chapter 6

Formal Analysis of Abnormal Excitation in Cardiac Tissue

We present the Piecewise Linear Approximation Model of Ion Channel contribution (PLAMIC) to cardiac excitation. We use the PLAMIC model to conduct formal analysis of cardiac arrhythmic events, namely Early Afterdepolarizations (EADs). The goal is to quantify (for the first time) the contribution of the overall sodium (Na^+), potassium (K^+) and calcium (Ca^{2+}) currents to the occurrence of EADs during the plateau phase of the cardiac action potential (AP). Our analysis yields exact mathematical criteria for the separation of the parameter space for normal and EAD-producing APs, which is validated by simulations with classical AP models based on complex systems of nonlinear differential equations. Our approach offers a simple formal technique for the prediction of conditions leading to arrhythmias (EADs) from a limited set of experimental measurements, and can be invaluable for devising new anti-arrhythmic strategies.

6.1 Introduction

An *action potential* (AP) is a change in an excitable cell's membrane potential caused by the flow of different ions across the cell membrane. The left panel in Fig. 29 illustrates a normal AP waveform for a guinea-pig heart cell. By convention, a normal AP follows a well defined cycle of "depolarization" (the rising phase),

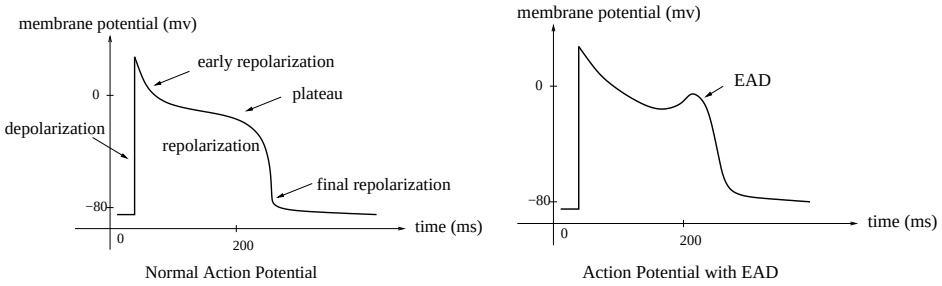

Figure 29: EAD in cardiac myocyte.

followed by “repolarization” (the falling phase). Furthermore, in qualitative terms, the “repolarization” phase can be divided in “early repolarization”, “plateau” and “final repolarization”.

Under some pathological conditions leading to a prolonged repolarization phase, the morphology of the AP can be altered by an abnormal secondary depolarization, termed **Early Afterdepolarization** (EAD). By clinical definition [19, 27], EADs occur before the completion of repolarization of an AP (as illustrated in the right panel of Fig. 29).

Such cellular-level events can give rise to undesired new excitation waves and can precipitate life-threatening heart activation sequences, e.g. tachyarrhythmias, especially in patients with Long QT syndrome [37, 41]. As critical arrhythmia triggers, EADs have been of interest to cardiac researchers for several decades [65]. Attempts have been made to uncover the ionic mechanisms underlying EADs, so that their occurrence can be predicted as well as effectively treated. Various studies have found that the reactivation of calcium (Ca^{2+}) or sodium (Na^{+}) channels or abnormally reduced potassium (K^{+}) current can lead to this phenomenon [16, 17, 39]. Yet, a unified view of EAD mechanisms along with predictive criteria are lacking.

In this paper, we present the *Piecewise Linear Approximation Model of the Ion Channel contribution* (PLAMIC) as a basis for understanding and analyzing the biochemical mechanisms underlying the formation of EADs during the cardiac action potential. The derivation of the PLAMIC model can be understood as follows. Let $V^{Na^{+}}$, $V^{Ca^{2+}}$ and $V^{K^{+}}$ denote the integral contributions to the AP due to the sodium, calcium and potassium channels, respectively; i.e. the voltages the ionic currents flowing through these channels induce. Further, let V^{NaK} denote the combined sodium and potassium voltage.

A key observation is that during normal and abnormal APs, the behavior of $V^{Ca^{2+}}$ and V^{NaK} corresponds to triangular-like functions of opposite polarity (see Fig. 31). As such, in the PLAMIC model, $V^{Ca^{2+}}$ and V^{NaK} are approximated in a piecewise-linear fashion using two very simple triangular functions, each of which naturally comprises a rising phase and a falling phase. The PLAMIC model also incorporates an AP-morphology-related (exponential) decay function, which can be fitted across different cell types.

A main advantage of the PLAMIC model then is its highly constrained parameter space, essentially limited to the peak voltage values and their occurrence in time of the two triangular functions. The model is therefore amenable to a closed-form, voltage-monotonicity analysis on the AP cycle during repolarization. We in fact show that the absence of a monotonically decreasing AP V ($\frac{dV}{dt} < 0$) during the plateau phase of repolarization is a necessary and sufficient condition for EAD. We furthermore provide specific conditions on the parameter space (involving the relative slopes of the two triangular functions, the relative occurrence of their peaks, and their relative magnitudes) for EAD occurrence.

We also performed an experimental validation of the conditions derived from the above-described formal analysis of the PLAMIC parameter space, assembling a test set of normal and abnormal APs from the widely accepted Luo-Rudy model ventricular cell model [46]. Our results demonstrate that the results of our formal analysis can be used as a valid classifier for EAD prediction.

The organization of the rest of the paper is as follows: Section 6.2 provides a formal definition of the PLAMIC model. Section 6.3 conducts a model-based analysis of the conditions under which EADs occur. Section 6.4 uses computer simulations with the Luo-Rudy model to validate our results. Section 6.5 offers our concluding remarks and directions for future work.

6.2 The PLAMIC Model

Mathematical modeling of excitable cells has a long tradition, starting with the first empirically-derived ionic model of the action potential in a giant squid axon proposed by Hodgkin and Huxley in 1952 [38]. Subsequently, more ion channels and complex biophysical processes have been included in these models, although

the general mathematical framework for representing the ion-channel contribution has remained essentially the same.

The model we propose adopts an abstraction based on voltage, i.e., it deals with the superposition of the voltages generated by the individual ion channels. We study the occurrence of EADs as a disturbance in the subtle balance between the underlying ion currents using their voltage surrogates.

The advantage of using superposition of the voltages, as opposed to the ionic currents directly, is the integral (smoother) nature of the former in the RC-circuit model that approximates the electrical behavior of the cell membrane. This facilitates the curve-fitting process and allows for simpler mathematical expressions to be employed and further linearized in a piecewise fashion. The result is the *Piecewise Linear Approximation Model of the Ion-Channel contributions* (PLAMIC).

We illustrate the idea of the PLAMIC model starting from a modification of traditional ionic models based on the Hodgkin-Huxley formalism. The main equation used in these ionic models is presented in Eqn. 21.

$$C\dot{V} = -\sum I_{\mathrm{i}}(t) + I_{\mathrm{st}}(t) \tag{21}$$

where $\dot{V}$ is the time derivative of the membrane potential V, C is the equivalent capacitance of the cell membrane, $\sum I_i(t)$ is the sum of all the ion currents flowing in or out of the cell membrane, and $I_{\mathrm{st}}(t)$ is the stimulation current.

$\sum I_i(t)$ may incorporate a number of individual currents for different cell types. For example, in the Luo-Rudy model [46] (LRd), a widely accepted ventricular cell model, currents can be grouped by ion species as in Eqn. 22.

$$\sum I_{\mathrm{i}}(t) = I_{\mathrm{Na}}(t) + I_{\mathrm{K}}(t) + I_{\mathrm{Ca}}(t) \tag{22}$$

where I_{Na}, I_{K}, and I_{Ca} are the sodium, potassium and calcium overall ion currents, respectively. The top row of Fig. 30 plots these three components of the LRd model for a normal AP.

Using for each component current the corresponding voltage, Eqns. 21 and 22 can be equivalently rewritten into the following form (Eqn. 23):

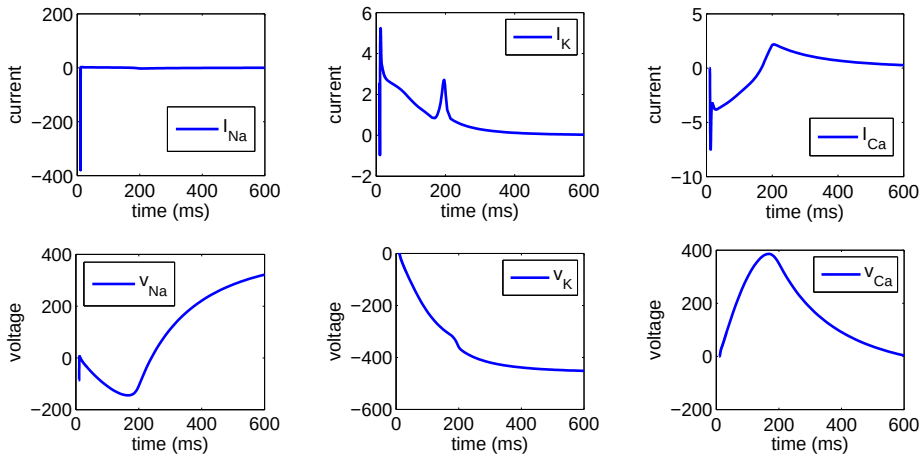

Figure 30: Individual ionic currents and their corresponding voltages in the LRd model.

$$\begin{aligned} C\dot{V}_{\mathrm{Na}} = -I_{\mathrm{Na}}(t), C\dot{V}_{\mathrm{K}} = -I_{\mathrm{K}}(t) \\ C\dot{V}_{\mathrm{Ca}} = -I_{\mathrm{Ca}}(t), C\dot{V}_{\mathrm{st}} = I_{\mathrm{st}}(t) \\ V = (V_{\mathrm{Na}}(t) + V_{\mathrm{K}}(t) + V_{\mathrm{Ca}}(t)) + V_{\mathrm{st}}(t) \end{aligned} \tag{23}$$

where V_{Na}, V_{K}, V_{Ca} and V_{st} are the voltages obtained via integration from I_{Na}, I_{K}, I_{Ca} and I_{st}, respectively.

The motivation behind Eqn. 23 is to first calculate the voltages from the individual currents and then obtain the overall membrane potential via superposition. Note the much smoother appearance of the voltage curves (bottom row) compared to the "spikey" current curves (top row) in Fig. 30. Furthermore, grouping the sodium and potassium voltages into one combined voltage yields the opposing triangular-like (and thus inherently linearizable) voltage functions depicted in Fig. 31.

The essentially triangular-shaped voltage functions suggests the use of two linear segments (linked together in a triangular form) to approximate the combination voltage due to the sodium and potassium currents (denoted as the N*aK* voltage), and the individual voltage due to the calcium current alone (the C*a* voltage).

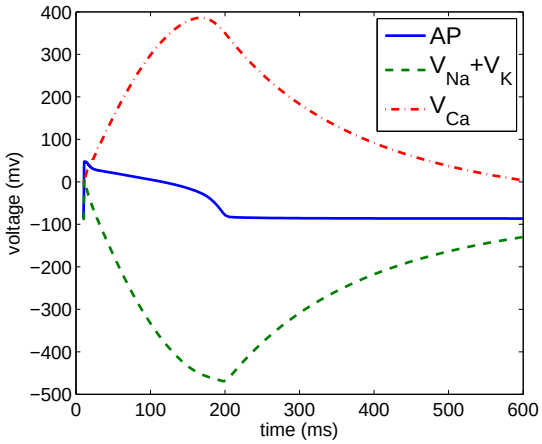

Figure 31: AP, combined sodium and potassium voltage, and calcium voltage in LRd model.

6.2.1 Definition of the PLAMIC Model

Two linear segments, forming a triangle (also known as a Lagrange hat function), are used to represent each of the N*aK* and C*a* voltages. Two of the triangle vertices (beginning and end) are fixed on the time-axis and the triangle shape varies by shift in the free (peak) vertex. The triangular function is shown in Fig. 32 (A). It is essentially a two-piece linear function starting from point $(0,0)$ and ending at $(T_S,0)$, where T_S is the total simulation time for the generation of an AP.

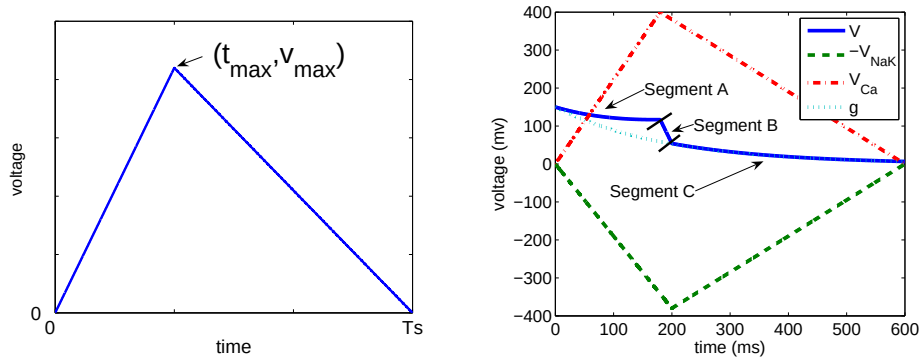

(A) The triangular function. (B) The PLAMIC model.

Figure 32:

By fixing the simulation time T_S, each function is determined solely by the

switching (peak) point $(t_{\max}, v_{\max})$. The mathematical definition of the triangular function is given by Eqn. 24, where the superscript $u \in \{\mathrm{Ca}, \mathrm{NaK}\}$ is used to distinguish the voltage functions corresponding to the different current types.

$$f^u(t) = \begin{cases} \frac{v^u_{\max}}{t^u_{\max}} t, & t \leq t^u_{\max}; \\ \\ \frac{T_S - t}{T_S - t^u_{\max}} v^u_{\max}, & t^u_{\max} < t \leq T_S. \end{cases} \tag{24}$$

The functions for v_{Ca} and v_{NaK} are then defined simply as follows:

$$v_{\mathrm{Ca}}(t) = f^{\mathrm{Ca}}(t) \tag{25}$$

$$v_{\mathrm{NaK}}(t) = f^{\mathrm{NaK}}(t) \tag{26}$$

The overall action potential v is the superposition of the two (Eqn. 27).

$$v(t) = v_{\mathrm{Ca}}(t) - v_{\mathrm{NaK}}(t) + g(t) \tag{27}$$

where $g(t)$ is a decay function related to the AP morphology. It is defined by $V_{\max}$, the absolute difference between the resting potential and the maximum voltage during upstroke, and by D ($D < 0$), an action-potential-duration parameter which can be adjusted across different cell types (Eqn. 28).

$$g(t) = V_{\max} e^{\mathrm{D}t} \tag{28}$$

The decay function qualitatively reflects the passive component of the cell-membrane response: an RC circuit will exhibit exponential decay after the upstroke due to capacitor discharge. In the PLAMIC model, this passive decay is used in conjunction with the superposed opposite potentials (NaK and Ca).

Based on the relative magnitude of $t^{\mathrm{Ca}}_{\max}$ and $t^{\mathrm{NaK}}_{\max}$ (i.e. which voltage reaches its peak first), the AP equation for v (Eqn. 27) has two alternative formulations. In each case, v is represented as a three-segment function, referred to in the following equations as segments A, B and C, respectively.

First, let $a^{\mathrm{c}}_1 = \frac{v^{\mathrm{Ca}}_{\max}}{t^{\mathrm{Ca}}_{\max}}$, $a^{\mathrm{c}}_2 = \frac{-v^{\mathrm{Ca}}_{\max}}{T_S - t^{\mathrm{Ca}}_{\max}}$, $b^{\mathrm{c}} = \frac{v^{\mathrm{Ca}}_{\max}}{T_S - t^{\mathrm{Ca}}_{\max}} T_S$, $a^{\mathrm{k}}_1 = \frac{v^{\mathrm{NaK}}_{\max}}{t^{\mathrm{NaK}}_{\max}}$, $a^{\mathrm{k}}_2 = \frac{-v^{\mathrm{NaK}}_{\max}}{T_S - t^{\mathrm{NaK}}_{\max}}$, and $b^{\mathrm{k}} = \frac{v^{\mathrm{NaK}}_{\max}}{T_S - t^{\mathrm{NaK}}_{\max}} T_S$.

Case I: $t_{\max}^{\mathrm{Ca}} < t_{\max}^{\mathrm{NaK}}$

$$v(t) = \begin{cases} a_1^{\mathrm{c}} t - a_1^{\mathrm{k}} t + V_{\max} e^{\mathrm{D}t}, & t \leq t_{\max}^{\mathrm{Ca}}, \text{ segment A;} \\ (a_2^{\mathrm{c}} t + b^{\mathrm{c}}) - a_1^{\mathrm{k}} t + V_{\max} e^{\mathrm{D}t}, & t_{\max}^{\mathrm{Ca}} < t \leq t_{\max}^{\mathrm{NaK}}, \text{ segment B;} \\ (a_2^{\mathrm{c}} t + b^{\mathrm{c}}) - (a_2^{\mathrm{k}} t + b^{\mathrm{k}}) + V_{\max} e^{\mathrm{D}t}, & t \geq t_{\max}^{\mathrm{NaK}}, \text{ segment C.} \end{cases} \tag{29}$$

Case II: $t_{\max}^{\mathrm{Ca}} \geq t_{\max}^{\mathrm{NaK}}$

$$v(t) = \begin{cases} a_1^{\mathrm{c}} t - a_1^{\mathrm{k}} t + V_{\max} e^{\mathrm{D}t}, & t \leq t_{\max}^{\mathrm{NaK}}, \text{ segment A;} \\ a_1^{\mathrm{c}} t - (a_2^{\mathrm{k}} t + b^{\mathrm{k}}) + V_{\max} e^{\mathrm{D}t}, & t_{\max}^{\mathrm{NaK}} < t \leq t_{\max}^{\mathrm{Ca}}, \text{ segment B;} \\ (a_2^{\mathrm{c}} t + b^{\mathrm{c}}) - (a_2^{\mathrm{k}} t + b^{\mathrm{k}}) + V_{\max} e^{\mathrm{D}t}, & t \geq t_{\max}^{\mathrm{Ca}}, \text{ segment C.} \end{cases} \tag{30}$$

In Fig. 32 (B), one of the possible implementations of the PLAMIC model (case I) is shown. The overall PLAMIC-abstracted AP is given as a solid line, with its three segments annotated accordingly. We plot $-v_{\mathrm{NaK}}$ instead of v_{NaK} to reveal the similarity to the LRd AP parameters shown in Fig. 31.

6.3 Formal Analysis of the PLAMIC Model

6.3.1 Monotonicity and EADs

EADs are secondary depolarization phenomena that arise during the repolarization phase; i.e. they disrupt the normal voltage return to rest. Therefore, a monotonicity analysis of the AP is an appropriate test for EADs. For example, it is safe to claim that a monotonically decreasing AP v ($\frac{dv}{dt} < 0$) is a sufficient condition for the absence of EADs. The opposite statement does not always hold, i.e. it is *not* always the case that if AP v is not universal decreasing, there is an EAD. For example, a "notch" in the early repolarization phase is common in many cardiac cells and is not considered an EAD (Fig. 33 (A)). Furthermore, in some cases, the membrane may transiently hyperpolarize; i.e. an undershoot may occur, with the potential lower than the resting potential during final repolarization. This non-monotonic case is also not an EAD (Figure 33 (B)).

If, however, the monotonicity analysis is restricted to the "plateau" phase of the repolarization process, any deviation from monotonic decay will effectively be an

(A) Notch during early repolarization. (B) Undershoot during final repolarization.

Figure 33: Non-monotonic APs that do not exhibit EADs.

EAD. In order to define the plateau phase in the PLAMIC model, let *notch-delay* be the cell-type-specific initial time segment of the repolarization phase during which a notch may occur. The PLAMIC plateau phase is then defined to consist of the suffix of segment A beginning at *notch-delay* followed by segment B. For most physiological choices of $(t^u_{\max}, v^u_{\max})$, $u \in \{\mathrm{Ca}, \mathrm{NaK}\}$, this definition of the plateau phase coincides closely with its physiological counterpart.

Based on the above monotonicity discussion, the following definition will serve as the theoretical basis of our formal analysis of EAD in the PLAMIC model.

Definition 1 *The PLAMIC model contains an* EAD *if* $\dot{v} > 0$ *at some point during the plateau phase.*

In Section 6.3.2, we present a monotonicity analysis of the PLAMIC plateau phase for both Cases I and II, and derive the exact conditions for EAD occurrence. Physiological explanations for these conditions are discussed as well.

6.3.2 Monotonicity Analysis of the PLAMIC Model

6.3.2.1 Case I

Case I is the most physiologically feasible scenario in cardiac cells. In simulation data of normal cardiac APs using the LRd model, $t^{\mathrm{Ca}}_{\max} < t^{\mathrm{NaK}}_{\max}$ holds at all times. As the PLAMIC-based voltage is a piecewise-linear function, monotonicity is analyzed on a per-segment basis.

Table 6: Summary of conditions for the existence of EAD in segment A.

Condition	EAD	No EAD
$a_1^{\mathrm{c}} < a_1^{\mathrm{k}}$		Fig. 34 (A)
$a_1^{\mathrm{k}} < a_1^{\mathrm{c}} < a_1^{\mathrm{k}} - V_{\max}D$	Fig. 34 (D)	Fig. 34 (C)
$a_1^{\mathrm{k}} - V_{\max}D < a_1^{\mathrm{c}}$	Fig. 34 (B)	

Segment A The first derivative of v within this segment is given by the following equation:

$$\frac{dv}{dt} = a_1^{\mathrm{c}} - a_1^{\mathrm{k}} + V_{\max}De^{\mathrm{Dt}} \tag{31}$$

Imposing the condition $\frac{dv}{dt} > 0$ yields:

$$t > \frac{1}{D}\ln(\frac{a_1^{\mathrm{k}} - a_1^{\mathrm{c}}}{V_{\max}D}) \tag{32}$$

Further examination of Eqn. 32 shows that the existence of a positive real solution for t requires the following conditions to hold:

$$\begin{cases} a_1^{\mathrm{c}} > a_1^{\mathrm{k}} > 0 \\ 0 < \frac{a_1^{\mathrm{k}} - a_1^{\mathrm{c}}}{V_{\max}D} < 1 \\ t < t_{\max}^{\mathrm{Ca}} \end{cases}$$

which are summarized in Theorem 2 as the major result for case I.

Theorem 2 $(a_1^{\mathrm{k}} < a_1^{\mathrm{c}} < (a_1^{\mathrm{k}} - V_{\max}D)) \wedge (t_{\max}^{\mathrm{Ca}} > \frac{1}{D}\ln(\frac{a_1^{\mathrm{k}} - a_1^{\mathrm{c}}}{V_{\max}D}))$ *is a sufficient condition for a case-I occurrence of EAD during the suffix of segment A beginning at notch-delay.*

In Fig. 34, we plot the different possibilities of the relative magnitudes of a_1^{k} and a_1^{c}. Table 6 summarizes the relationship between these values and the occurrence of EAD.

An intuitive physiological explanation of the above result is that the existence of EAD is closely related to the relative speeds of the voltage increase due to different ion currents, represented by a_1^{c} and a_1^{k}.

At the beginning of the plateau phase, the AP follows a decreasing trend, which requires the calcium current to have an upper bound ($a_1^{\mathrm{c}} < a_1^{\mathrm{k}} - V_{\max}D$); otherwise,

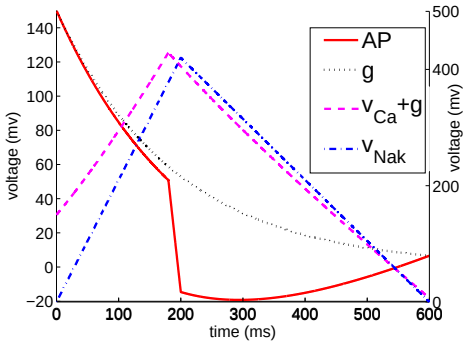

(A) $a_1^c < a_1^k$, no EAD

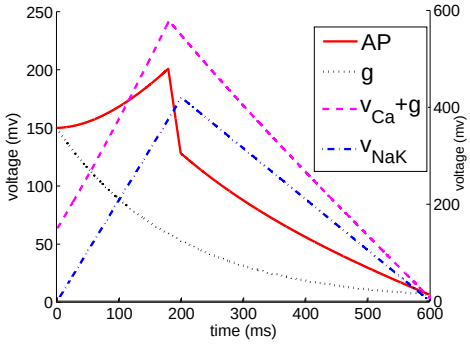

(B) $a_1^k - V_{max}D < a_1^c$, EAD

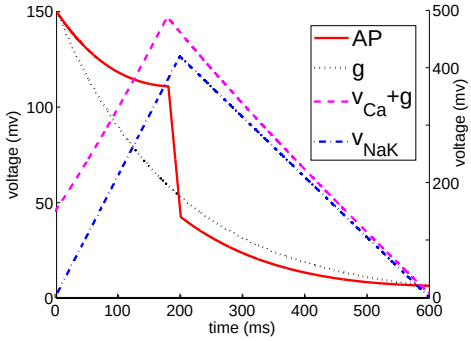

(C) $a_1^k < a_1^c < a_1^k - V_{max}D$ and $t_{max}^{Ca} \leq \frac{1}{D}\ln(\frac{a_1^k - a_1^c}{V_{max}D})$
No EAD

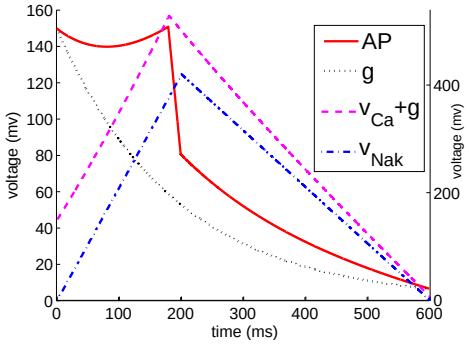

(D) $a_1^k < a_1^c < a_1^k - V_{max}D$ and $t_{max}^{Ca} > \frac{1}{D}\ln(\frac{a_1^k - a_1^c}{V_{max}D})$
EAD

Figure 34: PLAMIC-based analysis for EAD occurrence in segment A. The AP and decay functions are plotted as solid lines and use the y-axis on the left; v_{NaK} and $v_{Ca} + decay$ are plotted in dashed lines and use the y-axis on the right. The same conventions apply to Figs. 35 and 36.

the AP curve will be increasing through this segment. Furthermore, for an EAD to form, the balance has to be in favor of the calcium-current contribution ($a_1^{\mathrm{k}} < a_1^{\mathrm{c}}$). The last condition ensures that the calcium current has enough time to accumulate for the formation of an EAD ($t_{\max}^{\mathrm{Ca}} > \frac{1}{D}\ln(\frac{a_1^{\mathrm{k}}-a_1^{\mathrm{c}}}{V_{\max}D})$).

Segment B As in the analysis for segment A, we first determine the expression for $\frac{dv}{dt}$:

$$\frac{dv}{dt} = a_2^{\mathrm{c}} - a_1^{\mathrm{k}} + V_{\max}De^{\mathrm{Dt}} \tag{33}$$

Since $\frac{dv}{dt} < 0$ throughout this segment ($a_2^{\mathrm{c}} < 0$, $-a_1^{\mathrm{k}} < 0$ and $V_{\max}De^{\mathrm{Dt}} < 0$), no EAD is possible in segment B.

6.3.2.2 Case II

The defining segment-A equation for v is exactly the same as in case I, modulo the replacement of $t_{\max}^{\mathrm{Ca}}$ with $t_{\max}^{\mathrm{NaK}}$ in the time bound for t. Following the case-I analysis for segment A, this observation yields the following condition for the occurrence of EADs:

$$\begin{cases} a_1^{\mathrm{c}} > a_1^{\mathrm{k}} > 0 \\ 0 < \frac{a_1^{\mathrm{k}}-a_1^{\mathrm{c}}}{V_{\max}D} < 1 \\ t < t_{\max}^{\mathrm{NaK}} \end{cases}$$

Similarly, the major result for Case II can be summarized as follows.

Theorem 3 $(a_1^{\mathrm{k}} < a_1^{\mathrm{c}} < (a_1^{\mathrm{k}} - V_{\max}D)) \wedge (t_{\max}^{\mathrm{NaK}} > \frac{1}{D}\ln(\frac{a_1^{\mathrm{k}}-a_1^{\mathrm{c}}}{V_{\max}D}))$ *is a sufficient condition for a case-II occurrence of EAD during the suffix of segment A beginning at notch-delay.*

For segment B, the first derivative of v is given by the following equation.

$$\frac{dv}{dt} = a_1^{\mathrm{c}} - a_2^{\mathrm{k}} + V_{\max}De^{\mathrm{Dt}} \tag{34}$$

As $a_1^{\mathrm{c}} > 0$ and $a_2^{\mathrm{k}} < 0$, and $a_1^{\mathrm{c}} - a_2^{\mathrm{k}} + V_{\max}De^{\mathrm{Dt}} > 0$ for typical values of $V_{\max}$ and C, we observe an increasing AP during this segment. Thus, by Definition 1,

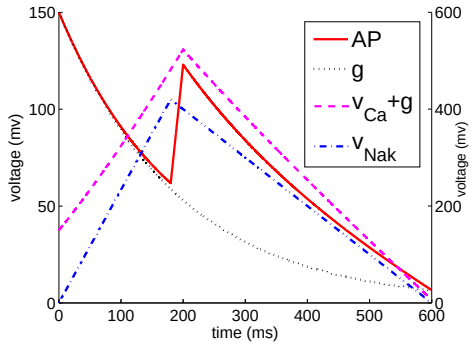

(A) Segment A has no EAD and Segment B has EAD.

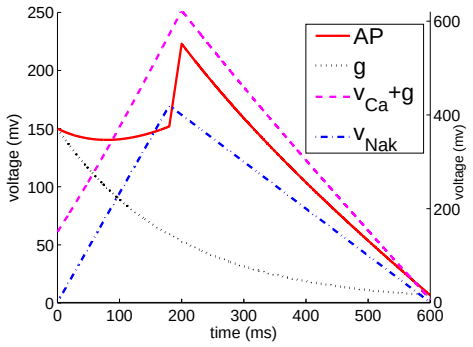

(B) Segments A and B both have EAD.

Figure 35: The existence of Case-II EAD for segment B.

segment B always has case-II EAD. Based on whether or not segment A has EAD, two cases are possible: EAD commences in (the tail end of) segment A or it commences in segment B; see Fig. 35.

Although this particular EAD morphology was not observed in the computer simulations we performed with the LRd model, this does not preclude its actual occurrence. Further examination of experimental data is needed to confirm or deny the physiological relevance of this case.

6.4 Experimental Validation of the PLAMIC Model

In this section, we consider the experimental validation of the PLAMIC model, specifically, the validity of Theorem 2 as an EAD predictor (classification rule) during the plateau phase of the AP cycle. To this end, we applied the protocols presented in [65] to the LRd cardiac-myocyte model to reproduce a number of AP curves with EADs. We also obtained the corresponding voltages for the calcium and the combined sodium and potassium currents using the integration method of Eqn. 23.

For each AP, in order to obtain the PLAMIC model parameters $(t^u_{\max}, v^u_{\max})$, $u \in \{\mathrm{Ca}, \mathrm{NaK}\}$, we took the maximum value of $V_{\mathrm{Na}} + V_{\mathrm{K}}$ as $v^{\mathrm{NaK}}_{\max}$, and the time at which it occurs as $t^{\mathrm{NaK}}_{\max}$. Data points $(t^{\mathrm{Ca}}_{\max}, v^{\mathrm{Ca}}_{\max})$ were obtained in a similar fashion. The constant coefficients in our experiments are defined as $V_{\max} = 150$, *offset*=127

(defined below), and $D = -0.0052$. These values have been chosen to match the LRd simulation results, but can be varied to fit different AP morphologies and cell types.

A side-by-side comparison of the AP curves obtained from the LRd and PLAMIC models for both normal and EAD-producing APs is illustrated in Fig. 36. The top-left panel shows a normal AP and an EAD-exhibiting AP, triggered by a calcium-current-enhancing drug, Bay K 8644. The top-right panel shows the PLAMIC model simulation for the two cases, which uses a piecewise-linear approximation of the current-inducing voltages obtained from the LRd model. The bottom row shows similar results for the LRd and PLAMIC models for EADs induced by the administration of cesium, resulting in a substantial prolongation of the repolarization phase.

The AP curves generated by the PLAMIC model qualitatively match the LRd curves, with an AP morphology that is more stylized due to the simplicity of the linear functions on which the PLAMIC model is based. Nevertheless, the EAD phenomenon and variations of the repolarization phase are well captured by the much simpler PLAMIC model.

To validate Theorem 2, formulated for the PLAMIC model, we need only focus on case I since the condition $t_{\max}^{\mathrm{Ca}} < t_{\max}^{\mathrm{NaK}}$ is always true in the LRd model. We also need to reformulate (the last condition of) Theorem 2 for the following reason. In the LRd model, v_{max}^{Ca}, the maximum value of V_{ca} during one AP cycle, serves as the sole contributor to the positive portion of the voltage. In the PLAMIC model, however, the positive part is composed of the linear function $v_{\mathrm{Ca}}(t)$ and the decay $g(t)$. Thus, when calculating the slope a_1^{c} in the LRd model, it is not accurate to use $v_{\max}^{\mathrm{Ca}}$ directly. Rather, a "decay" factor given by $V_{\max} e^{D t_{\max}^{\mathrm{Ca}}}$ should be subtracted from $v_{\max}^{\mathrm{Ca}}$.

The reformulation of Theorem 2 is given in Eqn. 35, where $\tilde{a}_1^{\mathrm{c}}$ is the corrected slope and *offset* is a constant used to ensure a non-negative AP value, as in the PLAMIC model.

$$
\begin{aligned}
& t_{\max}^{\mathrm{Ca}} > \tfrac{1}{D} \ln\left(\tfrac{a_1^{\mathrm{k}} - \tilde{a}_1^{\mathrm{c}}}{V_{\max} D}\right) \\
& \text{where } \tilde{a}_1^{\mathrm{c}} = \tfrac{v_{\max}^{\mathrm{Ca}} + \mathit{offset} - V_{\max} e^{D t_{\max}^{\mathrm{Ca}}}}{t_{\max}^{\mathrm{Ca}}} \\
& a_1^{\mathrm{k}} = \tfrac{v_{\max}^{\mathrm{NaK}}}{t_{\max}^{\mathrm{NaK}}}
\end{aligned}
\tag{35}
$$

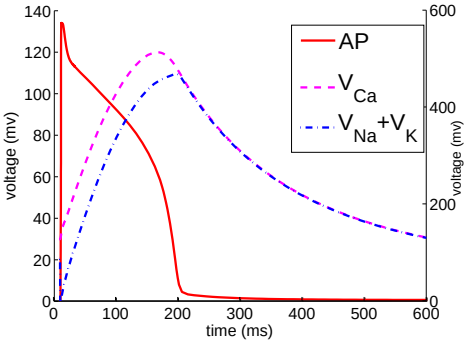

(A) Normal AP from LRd model.

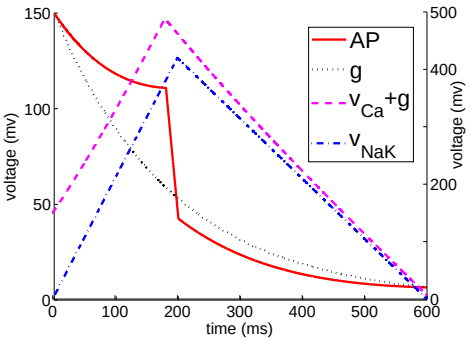

(B) Normal AP from PLAMIC model.

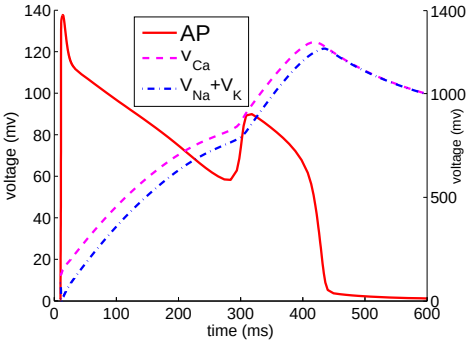

(C) EAD caused by Bay K 8644.

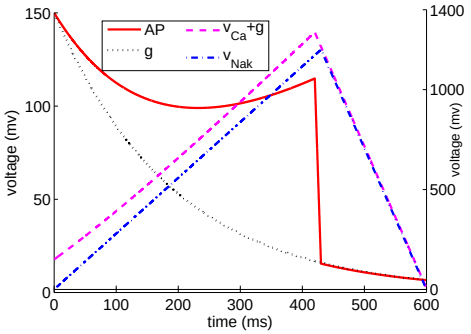

(D) EAD from PLAMIC model.

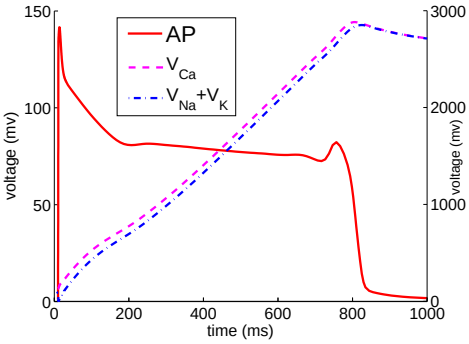

(E) EAD caused by cesium.

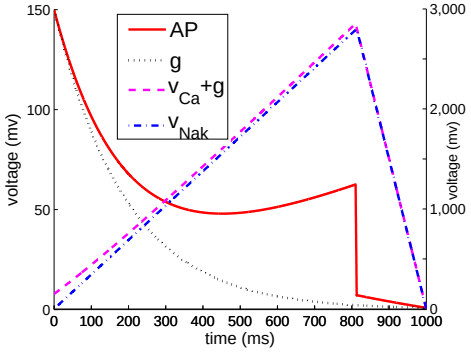

(F) EAD from PLAMIC model.

Figure 36: Comparison of AP curves from LRd and the PLAMIC model

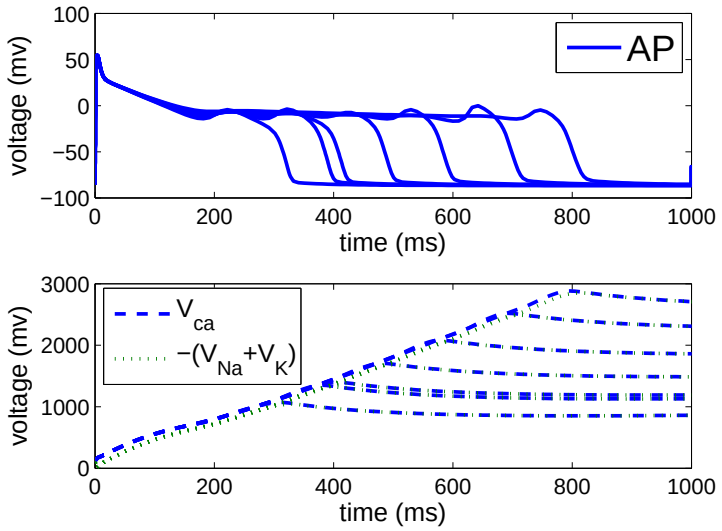

Figure 37: Simulation of normal AP and APs including EAD with variable timing and severity.

In order to test the validity of the derived condition for EAD occurrence given by Eqn. 35, we have assembled a test suite of LRd simulation data consisting of one normal AP and seven APs with variable EADs. The simulation results for both normal AP and abnormal APs are presented in Fig.37. The top panel shows the AP curves and the bottom panel shows $-(V_{\mathrm{Na}}+V_{\mathrm{K}})$ and V_{Ca} as defined by Eqn. 23.

Let $T_{\max}^{\mathrm{Ca}} \equiv \frac{1}{D}\ln(\frac{a_1^{\mathrm{k}}-\tilde{a}_1^{\mathrm{c}}}{V_{\max}D})$ be the *threshold value* for the LRd model. That is, according to Def. 1 and Thm. 2, an LRd AP should be EAD-producing if and only if $t_{\max}^{\mathrm{Ca}} > T_{\max}^{\mathrm{Ca}}$.[1] Note that since C and $V_{\max}$ are fixed for the LRd model, $T_{\max}^{\mathrm{Ca}}$ is a function of $a_1^{\mathrm{c}} - \tilde{a}_1^{\mathrm{k}}$, the slope difference.

For each AP, we calculate $a_1^{\mathrm{c}} - \tilde{a}_1^{\mathrm{k}}$ using the data points $(t_{\max}^u, v_{\max}^u)$, $u \in \{\mathrm{Ca}, \mathrm{NaK}\}$, obtained via numerical simulation from the LRd model, and calculate the threshold time $T_{\max}^{\mathrm{Ca}}$ derived from our formal analysis. This allows us to then compare the $t_{\max}^{\mathrm{Ca}}$ values with the $T_{\max}^{\mathrm{Ca}}$ values. The results of these comparisons are given in Fig. 38, where we plot $t_{\max}^{\mathrm{Ca}}$ and $T_{\max}^{\mathrm{Ca}}$ as a function of the slope difference $a_1^{\mathrm{c}} - \tilde{a}_1^{\mathrm{k}}$.

[1] The other conditions required by Theorem 2 for EAD occurrence, $a_1^{\mathrm{k}} < a_1^{\mathrm{c}} < (a_1^{\mathrm{k}} - V_{\max}D)$, are needed to ensure the existence of a positive real solution for t and are not considered here.

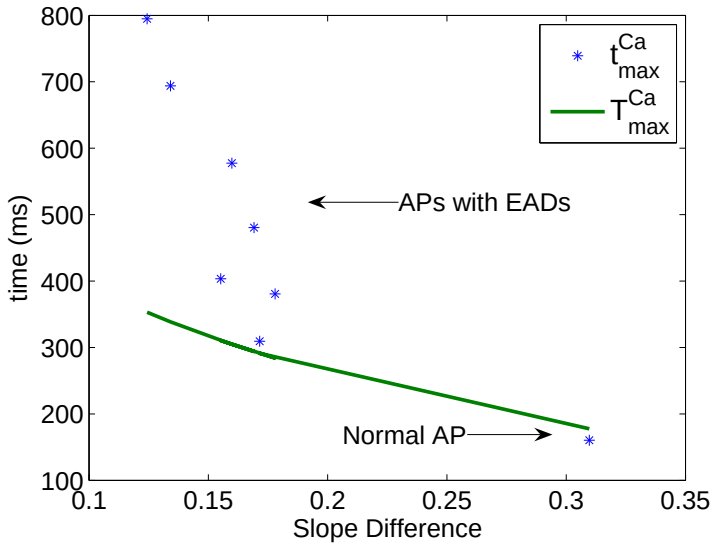

Figure 38: Validation of the Theorem 2 classification rule for EADs.

As can be seen in Fig. 38, for all APs with EAD, we have that $t^{\text{Ca}}_{\text{max}} > T^{\text{Ca}}_{\text{max}}$. Conversely, for all APs without EAD (only one such AP in our data set), $t^{\text{Ca}}_{\text{max}} < T^{\text{Ca}}_{\text{max}}$. Physiologically, these results suggest that the cells generating EADs spend an amount of time greater than the threshold in letting calcium accumulate and thereby dominate the effects of repolarizing potassium in order to produce such abnormal secondary depolarization. Regardless of the underlying physiology, the results of Fig. 38 demonstrate that Theorem 2 can be used as a valid classifier for EAD prediction, as suggested by the formal analysis.

6.5 Conclusions

In this chapter, we presented the PLAMIC model, a new, simplified model of the action potential in excitable cells. Despite its simplicity and piecewise-linear nature, the PLAMIC model preserves ties to main ionic species and the time course of their contributions to the AP. This allowed us to analyze biological phenomena of clinical importance: early afterdepolarizations (EADs). Unlike the original, highly nonlinear system of equations typically used to model an AP, the PLAMIC model proved amenable to formal analysis.

Specifically, with the PLAMIC model, we were able to explore the parameter space, without having to rely on exhaustive simulations, and to derive basic rules for the conditions under which EADs may occur. Overall, such conditions relate to the subtle balance of different ionic currents during the plateau phase of the repolarization process. While this result is somewhat intuitive and not surprising, to the best of our knowledge, our study is the first to formalize it and to provide quantitative rules for prediction of normal and EAD-containing APs based on the abstracted representation of the contributing ionic currents. We successfully validated the classification rules obtained by formal analysis with the PLAMIC model by computer simulations with widely accepted, detailed nonlinear AP models.

The utility of the PLAMIC model is rooted in its direct links to experimentally measurable parameters, and the relatively easy derivation of the EAD classification rules for a wide range of AP shapes and different cell types and species. Such a prediction tool can be very useful in designing new anti-arrythmic therapies and in confirming the safety of any genetic or pharmacological manipulations of excitable cells that may lead to alterations in the balance of ionic currents.

There are several limitations of the PLAMIC model. First, due to its simplicity, the AP curves are only qualitatively reproduced. Second, as the PLAMIC model studies the *overall contribution* of an ionic current to changes in the AP; details about the components of a current (steady-state behavior, kinetics parameters), which may be important, are lacking. For example, calcium handling constitutes an important aspect of cardiac-cell function, especially with regard to electromechanical coupling. Our model only indirectly reflects the effects of intracellular calcium on the action potential (AP). In particular, with $V_{\mathrm{Ca}}(t)$, we have modeled the integral contribution of calcium fluxes to the AP. In the Luo-Rudy model, for example, this term would correspond to the sum of the L-type Ca^{2+} channel (which has a Ca^{2+} sensitive gate), the Na/Ca exchanger and the background Ca^{2+} current. By qualitatively capturing the behavior of the Luo-Rudy model, especially with respect to monotonicity in the post-upstroke AP, we indirectly take into account changes in intracellular Ca^{2+}, although the PLAMIC model lacks parameters directly associated with these changes. While developing the model, our goal was to maintain simplicity so that monotonicity analysis could be performed on its parameter space for EAD-predictive purposes; as such, the PLAMIC model focuses on transmembrane

fluxes only.

Future work includes validation of the PLAMIC model using actual experimental data with relevant statistical measures. Furthermore, we will explore the derivation of a more accurate excitable-cell model for EAD prediction, yet one that retains the possibility of formal analysis. Our work in using hybrid automata to model excitable cells [63] is one possible formal framework for this research direction.

Chapter 7

A Rational CLHA Model

We present the rational cycle-linear hybrid automata model (rCLHA) of ion currents contribution to excitation of cardiac cells. It is the first model that provides both accurate reproduction of action potential morphology, APD restitution and the possibility of formal analysis of abnormal excitation like early afterdepolarization (EAD).

7.1 Introduction

Designing an efficient and accurate model of excitation of cardiac cells is invaluable for studying the excitation phenomena, large-scale simulation and devising new strategies to prevent arrythmia. Most existing ionic models [9, 46] are highly nonlinear systems which can reproduce cardiac cell excitation dynamics but lack the ability to analyze and slow for simulation. Simplified models [14, 25, 50] are usually faster but still lacks the analytic power, its description of the physiological details like current changes are indirect and qualitative.

The CLHA model in Chapter 3 captures the action potential (AP) morphology, APD restitution, and provided faster simulation up to 8 folds speedup. It had 3 state variables, 4 modes and 1 memory variable which stayed constant in a given cycle. The CLHA model when associated with techniques as optimization and parallel computation, would fundamentally improve the simulation efficiency.

The limitation of our CLHA model is that as it lacks the biophysical details

about ion concentration and ionic currents, it will be unable to provide insights about the connection between AP morphology and the underlying ionic currents dynamics. To address this problem, we propose in this paper the rational CLHA model (rCLHA) which includes the details of ionic currents while keeping the system minimal. Further from CLHA model, the rCLHA model can provide a formal prediction of the existence of early afterpolarization (EAD) (PLAMIC model can do this analysis but can not reproduce AP morphology and restitution).

In this work, we explain the theory and method to construct the rCLHA model, then it is compared with previously published Luo-Rudy dynamic model (LRd). The rCLHA model is not for LRd model only, with proper parameter fitting, it can match the AP morphology and restitution from other cardiac cell models (or experiment data).

The organization of this chapter is as follows: Section 7.2 describe the rCLHA model and the connection between its parameters with the shape of AP. Section 7.3 presents the AP comparison and APD restitution with Luo-Rudy dynamic model. At last the discussion and future works are presented.

7.2 Methods

7.2.1 State Variables

The goal of rCLHA model is to use minimal number of state variables to capture as many biophysical details as it can. Traditionally, membrane potential and gating variables compose the major part of an ionic model. However, as the number of gating variables grows fast as the complexity of the system increases, it is impossible to capture all the dynamics of them in a simplified system. Instead, in the rCLHA model, we use four variables to represent the state of a cell system:

membrane potential v. This is the fundamental role in an excitable system.

Combined sodium and potassium current I_{NaK}. Sodium and potassium currents affect the shape of an AP at two distinct time period. It is believed that the fast upstroke is due to the sodium current and relative long plateau phase is caused by the activation of potassium current. Combination of these two

current will reduce the number of the variables while keeping the ability to discriminate them at different time point.

Calcium current I_{Ca}. Calcium current is important for both the physiological and electromechanical coupling of cardiac cells. It is widely accepted that the strength of calcium current in the repolarization phase determines the occurrence of arrythmia (EADs).

Timing variable w. This variable is going to determine the length of plateau, thus play an important role in the APD restitution property.

7.2.2 rCLHA Structure

In the previous CLHA model, we have discuss the method used to construct the modes in the hybrid automata. Especially, the physiologically defined phases (**Upstroke**, **Early Repolarization**, **Plateau**, **Final Repolarization**, **Resting** and an artificial **Stimulated** mode which is used to tell the existence of an external stimulus) are used as a guideline. In the rCLHA model, we define modes based on the different dynamics of two state variables $I_{\mathrm{N}aK}$ and $I_{\mathrm{C}a}$. Particularly, we associate a hybrid automaton model for each of them.

The plotting and modes for $I_{\mathrm{N}aK}$ is shown in Fig. 39 (Data using LRd model). As the magnitude changes fast, we plot the smaller current separately. As sodium and potassium currents affect AP shape at different time period, we assume the mode **Upstroke** describes Na current dynamics and the other modes describes K current dynamics.

$I_{\mathrm{C}a}$ is illustrated in Fig. 40. The Ca current plotted is the combination of different types of Ca currents: L-type, exchanger, etc. The abstraction enable us to study Ca current as one entity and restricts the parameter space to a minimal set.

7.2.3 State Equations

The benefit of a linear model is obvious. It not only reduces the complexity of the system, but also opens to the possibility of control and analysis. The principle of the rCLHA model is to use piecewise linear system plus finite control (mode switches) to simulate the behavior of a nonlinear system. At the same time, the

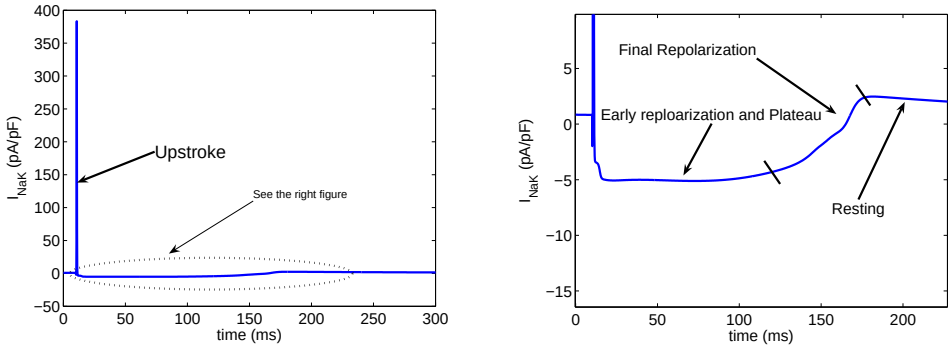

(A)Combined Na and K currents. (B)Detailed Na and K currents.

Figure 39: Combined Na and K currents and the modes classification.

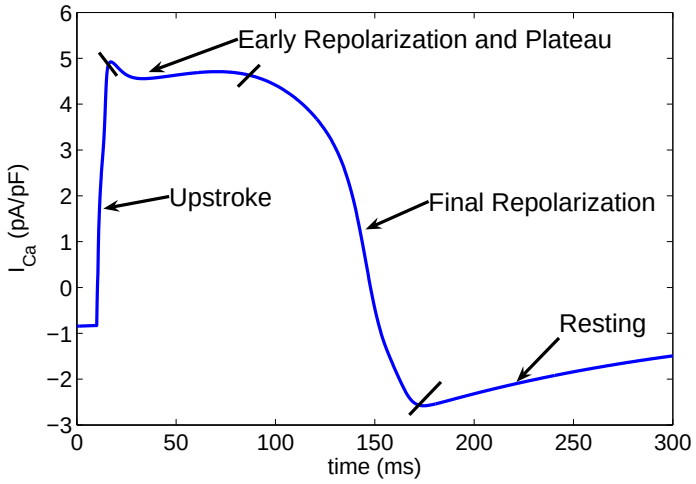

Figure 40: Ca currents and the modes classification.

physiological and physical laws are observed as well. Especially, the state equations is in the following form:

$$\dot{\overrightarrow{X}} = A\overrightarrow{X} + B \tag{36}$$

$$\tag{37}$$

Where $\overrightarrow{X} = (v, I_{\mathrm{NaK}}, I_{\mathrm{Ca}}, w)^T$ is the vector of state variables, A is a 4×4 constant matrix and B is a 4×1 constant vector. In most modes, A is in the following form (exceptions will be explained later):

$$\begin{pmatrix} 0 & 1 & 1 & 0 \\ 0 & a_1 & 0 & 0 \\ 0 & 0 & a_2 & 0 \\ 0 & 0 & 0 & 0 \end{pmatrix} \tag{38}$$

and $B = (0, b_1, b_2, b_3)^T$, where a_1, a_2, b_1, b_2, b_3 are constants.

The ideas behind the above design is explained below.

$\dot{v} = I_{\mathrm{NaK}} + I_{\mathrm{Ca}}$:

This is consistent with the physical law which defines the change of voltage of a plane capacitor which is widely used to model excitable cell membrane. One of the assumptions is that the capacitor is constant 1. To keep the equation simple, we remove the negative sign in front of the sum of the membrane currents. Accordingly, the plotting of the currents are reversed with sign as well.

$\dot{I_{\mathrm{NaK}}} = a_1 I_{\mathrm{NaK}} + b_1$:

With different choice of a_1 and b_1, I_{NaK} will take different shape. Noticed that, it is not necessary that the system stays stable in all modes. Actually, it is proved that the **Upstroke** mode, there is a positive feedback loop: $depolarization \rightarrow Nachannelactivation \rightarrow depolarization$, and it is considered crucial for the excitation of cells. The equation also shows that the current will change independently which is an abstraction of the current dynamics where voltage v also influence the shape of current.

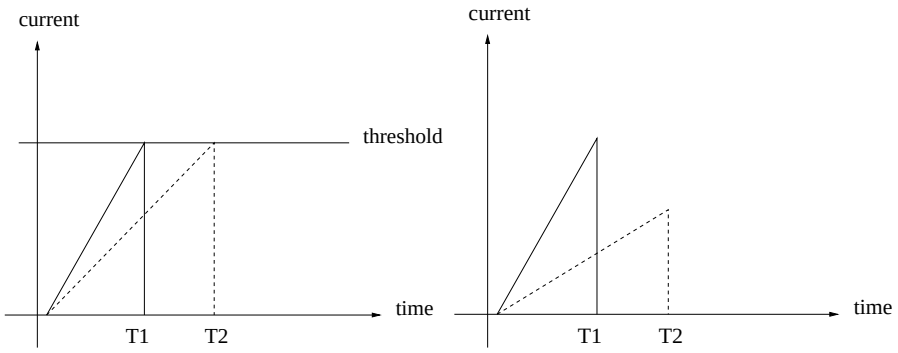

Figure 41: (A)Current as threshold. (B) Voltage as threshold.

$\dot{I_{\text{Ca}}} = a_2 I_{\text{Ca}} + b_2$:

Similar to the idea above.

$\dot{w} = b_3$:

The change of the timing variable is approximated by a ramp function for simplicity.

7.2.4 Parameter justification and fitting

We then explain how parameters a_1, a_2, b_1, b_2, b_3 influence the shape of AP mode by mode.

Upstroke This is the major depolarization phase. In this phase, Na gate opens fast and the positive feedback between the activation of Na currents and the voltage depolarization enables both Na current and voltage v reaching threshold immediately. This fast dynamics is approximated by a positive and large value of a_1 which results an exponential increase in both NaK current and voltage.

However, small perturbation of parameters a_1 will result a large change in the value of NaK current or voltage v, based on the manner that the hybrid automata switches the mode.

If mode switch is defined as current reaches threshold, a smaller a_1 will result a larger voltage v. If the switch is defined by the time when voltage v reaches the threshold, a smaller a_1 will give a smaller NaK current. It is illustrated in Fig. 41.

NaK current is approximated by a linear function with time. Two linear functions are plotted in solid line and dashed line which represents functions with larger a_1 and a small a_1 respectively. In case (A) where mode switches when current reaches threhold, the solid line reaches threshold at T_1 and the dashed line reaches threshold at time T_2. The area enclosed by the two functions represents the value of voltages which are the integration of the currents. It is obvious that a slower current will result a larger voltage. In case (B), the voltage (area below the line) will be the same for both fast and slow current functions, the slower function will reach a lower value at the point where switch happens.

In the current implementation of rCLHA, we adopt the first case where we use current value to control the switch of modes.

Early repolarization and plateau We use linear time-invariant systems to simulate the dynamics of NaK and Ca current dynamics in mode **Early repolarization** and **Plateau**. The justification is that both of them reach to a stable state at plateau as shown in Fig. 39 and Fig. 40. From the state equation of NaK and Ca current, the stable values are

$$\tau_1 = -b_1/a_1 \tag{39}$$

$$\tau_2 = -b_2/a_2 \tag{40}$$

where τ_1 is around -5.1 pA/pF for NaK current and τ_2 is around 4.5 pA/pF for Ca current. The absolute value of NaK stable current is greater than that of Ca current to enforce a repolarization phase reflected in the value of voltage v.

The shape of AP at early repolarization phase is determined by the absolute value of a_1 and a_2 and the time point when switch from Upstroke to Early repolarization happens for the hybrid automaton for both NaK and Ca current. For example, the notch (Fig. 42) which is a usual phenomenon for many cardiac cells. In the rCLHA simulations, if the automata for NaK and Ca switch from Upstroke to Early repolarization at the same time, it can be proved that there is no “notch” happening. If NaK switches to Early repolarization earlier than Ca current, with certain combination of a_1 and a_2, “notch” will occur. (More details later)

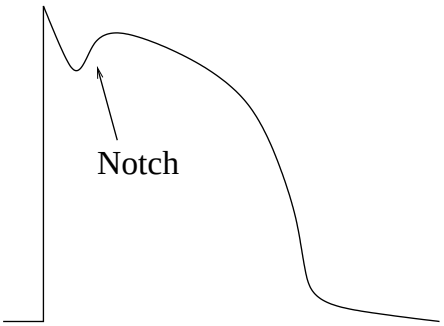

Figure 42: Notch at the early repolarization phase.

As both NaK and Ca currents approaches to the stable value at the end of this phase, the system becomes very sensitive to the threshold value if we still use threshold to control the mode switch. The solution is to use the timing variable instead of the NaK and Ca current themselves to determine when the switch should take place.

The timing variable *w* will follow a linear increase. The speed is determined by a memory variable which we will explain further in subsection 7.2.5. Intuitively, the faster it increases, the sooner it reaches the threshold and the shorter the plateau phase, which will result a short action potential duration (APD).

Final repolarization In this mode, NaK current increases from -5 pA/pF to 2.5 pA/pF and Ca current decreases from 4.7 pA/pF to -2.7 pA/pF , as shown in Fig 39 and Fig. 40. Arrythmia might occur due to the imbalance of NaK and Ca current in this phase. A detailed analysis for the existence of arrythmia (EADs) based on the parameter space will be presented in Section 6.3.

Resting This is the last phase of an AP cycle. Both NaK and Ca current follow a slow exponential decreasing function to 0 in this mode. The AP shape is very sensitive to the decreasing speed of both current as the value is closed to the resting potential. Furthermore, as LRd model is known for the long term inaccuracy at the resting phase, an additional term is added to the dynamic function of *v* as follows to correct the above effects:

$$\dot{v} = I_{\text{NaK}} + I_{\text{Ca}} - 0.1(v + 86); \tag{41}$$

The last term in Equation 41 adds a strong converging factor to the value of v such that the over-sensitivity is reduced and possible oscillation is avoided.

Stimulated This is an artificial mode which represents the existence of an external stimulus current. The switch to this mode is triggered by an external event E_{on} which is an abstraction of the occurrence of stimulation. The equation for $\dot{v}$ thus becomes:

$$\dot{v} = I_{\mathrm{NaK}} + I_{\mathrm{Ca}} + I_{\mathrm{st}} \tag{42}$$

The other equations will stay the same with Resting mode. When another external event E_{off} happens, the current value of v is compared with a preset threshold T. When $v > T$, mode is switched to **Upstroke**, else, it switches to **Resting**.

7.2.5 Modeling APD restitution

It is widely believed that the excitable cells exhibit memory mechanism in the excitation behavior. Especially, when the pacing frequency increases, the cell will have a shorter APD. Instead of the nonlinear functions in a traditional ionic model to enforce the memory effect, we use a memory variable in rCLHA model to explicit "record" how soon a cell gets the second stimulation from the last one.

Especially, we use the value of I_{Ca} at the point of second stimulation occurs to control the value of a_1, a_2, b_1, b_2, b_3 at different AP cycles. As shown in the previous section, I_{Ca} is around -2.6 pA/pF at the beginning of Resting mode (Fig. 40). The closer this value to 0, the more complete the cell has recovered and a longer APD it will generate for the next excitation. A normalized value θ ($0 < \theta \leq 1$) is defined as follows:

$$\theta = (I_{\mathrm{Ca}} / -2.6) \tag{43}$$

Now a_1, a_2, b_1, b_2, b_3 become functions of θ, which is defined in Table 7.

At the beginning of mode **Early Repolarization and Plateau**, timer w is set to 0. And the time period spent in this mode is defined as

$$80 - 70\theta^2 \tag{44}$$

	a_1	b_1	a_2	b_2	b_3
UP	$16-8\theta$	0	0	$1.9+0.2\theta$	0
EP	-5	$-5(5.1+1.1\theta)$	-0.2	$0.2(4.66+\theta)$	1
FR	0.029	$0.029(5.77+1.1\theta)$	0.045	$-0.045(5.0+\theta)$	0
RT	-0.0038	0	-0.004	0	0
ST	-0.0038	0	-0.004	0	0

Table 7: Definition of the parameters. (UP: Upstroke; EP: Early repolarization and plateau; FR: Final repolarization; RT: Resting; ST: Stimulated.)

Thus, by changing the parameters or function in equation 44, we can match restitution curves for cardiac cells of different locations or species.

7.3 Result

The difference between rCLHA model and other ionic model is that it is not designed to reproduce every ion channel current, but to capture the AP morphology and restitution properties by using the sum of sodium, calcium and potassium currents. It turns out that this structure is sufficient for the task. With proper parameter fitting, it can replicate accurately the AP shape and retitution curves from other ionic models. In this section, we show that the parameter defined in last section can reproduce the AP and restitution curves from LRd model.

7.3.1 Action Potential Morphology

The AP curve from LRd shown is after pacing to steady state at a cycle length of 500 ms. The resting potential is -86 mV. The threshold for activation is set to -46 mV. The comparison is shown in Fig. 43.

7.3.2 Restitution Curve Comparison

The restitution is calculated using S1S2 protocol. It is measured by pacing at a specific cycle length (500 ms) until steady state then introducing second pulse over a range of intervals. The comparison of the APD (90%) restitution curve is in Fig. 44.

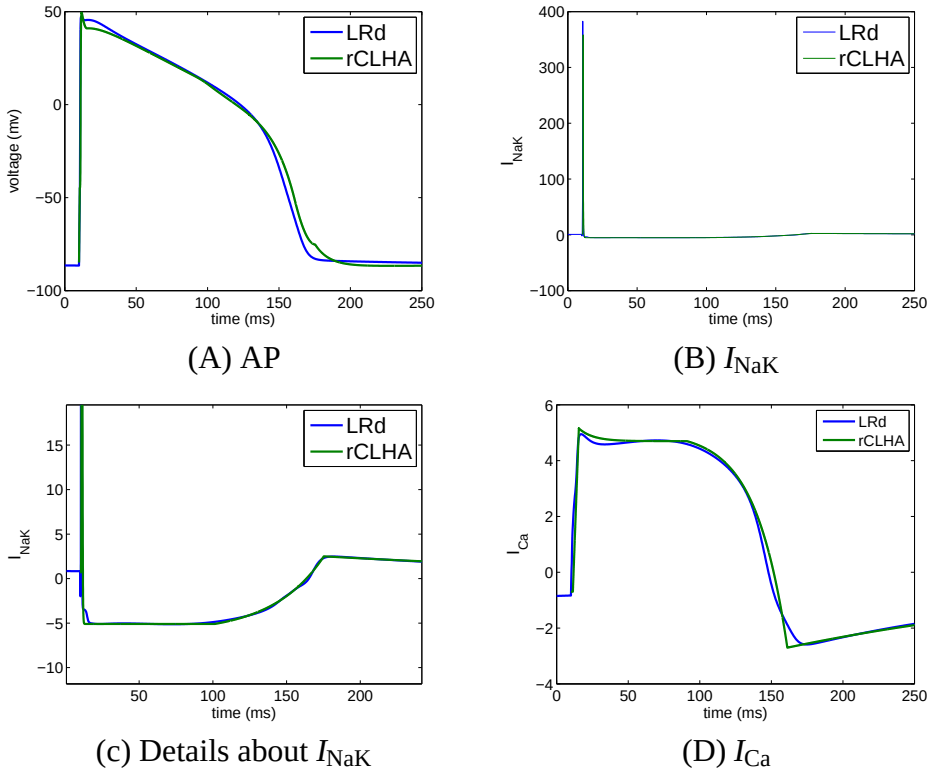

Figure 43: Fitting LRd using rCLHA model.

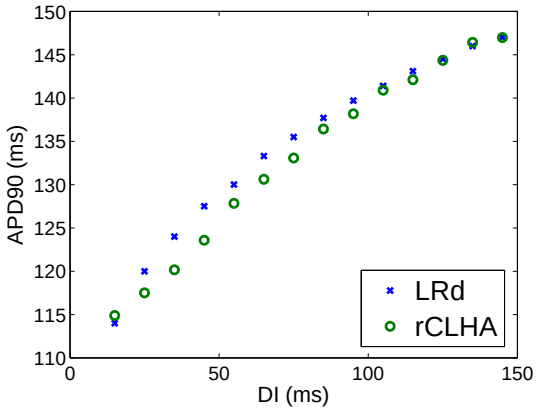

Figure 44: Comparison of APD restitution curves.

7.4 Discussion

In this chapter we introduce the rational CLHA model for the excitation of cardiac cells. This model is attractive for the following reasons: first, it is a simple model with only 4 state variables, which makes it is efficient in large scale simulations. Second, it keeps enough structure to study the relationship between the ionic currents and AP morphology, where most simplified models lack the quantitative reproduction of dynamics of currents. Third, the simple control of memory variable of rCLHA provides a new method to model restitution curves. Instead of using complex nonlinear functions, we can use piecewise linear system to reproduce the nonlinear property of excitation behavior. The last but not least benefit of a linear model is that it provides the possibility of mathematical analysis of the state space.

Future work includes improving the model to include more features like conduction velocity restitution and spatial simulation of propagation waves. From the analysis part, explore the parameter space for abnormal excitation events like early afterdepolarization (EADs). Thus rCLHA can be used to design new anti-arrythmia strategies.

Bibliography

[1] *MATLAB Online Reference Documentation*. http://www.mathworks.com/access/helpdesk/help/toolbox/optim/.

[2] R. Alur, C. Belta, F. Ivancic, V. Kumar, M. Mintz, G. Pappas, H. Rubin, and J. Schug. Hybrid modeling and simulation of biomolecular networks. In *Hybrid Systems: Computation and Control, HSCC 2001*, volume 2034 of *LNCS*, pages 19–32, 2001.

[3] R. Alur, T. Dang, and F. Ivancic. Reachability analysis of hybrid systems via predicate abstraction. In *HSCC*, pages 35–48, 2002.

[4] R. Alur and D. Dill. A theory of timed automata. *Theoretical Computer Science*, 126:183–235, 1994.

[5] R. Alur, R. Grosu, Y. Hur, V. Kumar, and I. Lee. Modular specifications of hybrid systems in CHARON. In *Hybrid Systems: Computation and Control, Third International Workshop*, volume LNCS 1790, pages 6–19, 2000.

[6] R. Alur, T. Henzinger, G. Lafferriere, and G. Pappas. Discrete abstractions of hybrid systems. *IEEE*, 89:971–984, 2000.

[7] A. Balluchi, L. Benvenuti, M. D. D. Benedetto, C. Pinello, and A. L. Sangiovanni-Vincentelli. Automotive engine control and hybrid systems: challenges and opportunities. *Proceedings of the IEEE*, 88(7):888–912, July 2000.

[8] P. Barbano, M. Spivak, J. Feng, M. Antoniotti, and B. Misra. A coherent framework for multi-resolution analysis of biological networks with memory:

Ras pathway, cell cycle and immune system. In *Proc. National Academy of Science*, volume 102, pages 6245–6250, 2005.

[9] G. W. Beeler and H. Reuter. Reconstruction of the action potential of ventricular myocardial fibres. *J Physiol*, 268:177–210, 1977.

[10] G. Behrmann, A. David, and K. Larsen. A tutorial on UPPAAL. In M. Bernardo and F. Corradini, editors, *Formal Methods for the Design of Real-Time Systems: 4th International School on Formal Methods for the Design of Computer, Communication, and Software Systems, SFM-RT 2004*, number 3185 in LNCS, pages 200–236. Springer–Verlag, September 2004.

[11] C. Belta, P. Finin, L. Habets, A. Halasz, M. Imielinski, V. Kumar, and H. Rubin. Understanding the bacterial stringent response using reachability analysis of hybrid systems. In *Hybrid Systems:Computation and Control, HSCC 2004*, volume 2993 of *LNCS*, pages 111–126, 2004.

[12] C. Belta, J. Schug, and T. Dang. Stability and reachability analysis of a hybrid model of luminescence in the marine bacterium vibrio fischeri. In *40th IEEE conference on Decision and Control*, volume 1, pages 869–874, 2001.

[13] A. Bemporad, A. Garulli, S. Paoletti, and A. Vicino. A bounded-error approach to piecewise affine system identification. *IEEE Transactions on Automatic Control*, 50(10):1473–1634, 2005.

[14] V. N. Biktashev. A simplified model of propagation and dissipation of excitation fronts. *International Journal of Bifurcation and Chaos*, 13:3605–3619, 2003.

[15] I. Biktasheva, R. Simitev, R. Suckley, and V. N. Biktashev. Asymptotic properties of mathematical models of excitability. *Philosophical Transactions of the Royal Society A: Mathematical Physical and Engineering Sciences*, 364:1283–1298, 2006.

[16] F. Charpentier, E. Drouin, C. Gauthier, and H. L. Marec. Early after/depolarizations and triggered activity: mechanisms and autonomic regulation. *Fundam Clin Pharmacol*, 7(1):39–49, 1993.

[17] W. Clusin. Calcium and cardiac arrhythmias: DADs, EADs, and alternans. *Crit Rev Clin Lab Sci*, 40(3):337–75, Jun 2003.

[18] M. Courtemanche, R. J. Ramirez, and S. Nattel. Ionic mechanisms underlying human atrial action potential properties: insights from a mathematical model. *Am J Physiol*, 275:301–321, 1998.

[19] P. F. Cranefield and R. S. Aronson. *Cardiac arrhythmias: the role of triggered activity and other mechanisms.* Futura Publishing Company, 1988.

[20] T. Dang. *Verification and Synthesis of Hybrid Systems*. PhD thesis, INPG, 2000.

[21] H. de Jong, J.-L. G. C. Hernandez, M. Page, T. Sari, and J. Geiselmann. Hybrid modeling and simulation of genetic regulatory networks: A qualitative approach. In *Hybrid Systems: Computation and Control, HSCC 2003*, volume 2623 of *LNCS*, pages 267–282, 2003.

[22] A. Deshpande, D. Godbole, A. Göllü, and P. Varaiya. Design and evaluation of tools for automated highway systems. In *Hybrid Systems III*, LNCS 1066, pages 138–148. Springer-Verlag, 1996.

[23] J. G. Dumas and A. Rondepierre. Modeling the electrical activity of a neuron by a continuous and piecewise affine hybrid system. In *Hybrid Systems: Computation and Control*, pages 156–171, 2003.

[24] T. Erbes. Stochastic learning feedback hybrid automata for dynamic power management in embedded systems, 2004.

[25] F. Fenton and A. Karma. Vortex dynamics in 3d continous myocardium with fiber rotation: Filament instability and fibrillation. *CHAOS*, 8:20–47, 1998.

[26] R. FitzHugh. Impulses and physiological states in theoretical models of nerve membrane. *Biophys J*, 1:445–467, 1961.

[27] H. Fozzard. Afterdepolarizations and triggered activity. *Basic Res Cardiol*, 87 Suppl 2:105–13, 1992.

[28] G.C.Rigatos, I. Vlahavas, and C. Spyropoulos. Fuzzy stochastic automata for reactive learning and hybrid control. In *Methods and Applications of Artificial Intelligence*, pages 366–377. LNCS, Vol. 2308, Springer-Verlag, 2002.

[29] R. Ghosh and C. J. Tomlin. Symbolic reachable set computation of piecewise affine hybrid automata and its application to biological modeling: Delta-notch protein signaling. *IEE Transactions on Systems Biology*, 1(1):170–183, June 2004.

[30] R. A. Gray and J. Jalife. Spiral waves and the heart. *Int J Bifurc Chaos*, 6:415–435, 1996.

[31] R. A. Gray, A. M. Pertsov, and J. Jalife. Spatial and temporal organization during cardiac fibrillation. *Nature*, 392:75–78, 1998.

[32] R. Grosu, S. Mitra, P. Ye, E. Entcheva, I. Ramakrishnan, and S. A. Smolka. Learning cycle-linear hybrid automata for excitable cells. In *Hybrid Systems: Computation and Control*, volume 4416 of *LNCS*, pages 245–258, Pisa, Italy, April 2007. Springer.

[33] M. M. Henry. Model-based estimation of probabilistic hybrid automata, 2002.

[34] T. Henzinger, P.-H. Ho, and H. Wong-Toi. Hytech: A model checker for hybrid systems. *Software Tools for Technology Transfer*, 1:110–122, 1997.

[35] T. A. Henzinger. The theory of hybrid automata. In *Proceedings of the 11th IEEE Symposium on Logic in Computer Science*, pages 278–293, 1996.

[36] T. A. Henzinger, P. W. Kopke, A. Puri, and P. Varaiya. What's decidable about hybrid automata. *Journal of Computer and System Sciences*, 57:94–124, 1998.

[37] M. Hiraoka, A. Sunami, F. Zheng, and T. Sawanobori. Multiple ionic mechanisms of early afterdepolarizations in isolated ventricular myocytes from guinea-pig hearts. *QT Prolongation and Ventricular Arrhythmias.*, pages 33–34, 1992.

[38] A. L. Hodgkin and A. F. Huxley. A quantitative description of membrane currents and its application to conduction and excitation in nerve. *J Physiol*, 117:500–544, 1952.

[39] N. Homma, M. Amran, Y. Nagasawa, and K. Hashimoto. Topics on the Na+/Ca2+ exchanger: involvement of Na+/Ca2+ exchange system in cardiac triggered activity. *J. Pharmacol Sci*, 102(1):17–21, 2006.

[40] M. Huber and R. Grupen. A hybrid architecture for learning robot control tasks. *Robotics Today*, 13(4), 2000.

[41] C. January and A. Moscucci. Cellular mechanism of early afterdepolarizations. *QT Prolongation and Ventricular Arrhythmias.*, pages 23–32, 1992.

[42] K. Joshi, N. Neogi, and W. Sanders. Dynamic partitioning of large discrete event biological systems for hybrid simulation and analysis. In *Hybrid Systems: Computation and Control, HSCC 2004*, volume 2993 of *LNCS*, 2004.

[43] G. Lafferriere, J. Pappas, and S. Yovine. A new class of decidable hybrid systems. In *HSCC*, pages 137–151, 1999.

[44] P. Lincoln and A. Tiwari. Symbolic systems biology: Hybrid modeling and analysis of biological networks. In *Hybrid Systems: Computation and Control, HSCC 2004*, volume 2993 of *LNCS*, pages 660–672, 2004.

[45] C. Livadas, J. Lygeros, and N. A. Lynch. High-level modelling and analysis of TCAS. In *Proceedings of the IEEE Real-Time Systems Symposium*, pages 115–125, 1999.

[46] C. H. Luo and Y. Rudy. A dymanic model of the cardiac ventricular action potential: I. simulations of ionic currents and concentration changes. *Circ Res*, 74:1071–1096, 1994.

[47] J. Lygeros, G. J. Pappas, and S. Sastry. An approach to the verification of the center-tracon automation system. In *HSCC '98: Proceedings of the First International Workshop on Hybrid Systems*, pages 289–304, London, UK, 1998. Springer-Verlag.

[48] O. Maler and S. Yovine. Hardware timing verification using KRONOS. In *7th IEEE Israeli Conference on Computer Systems and Software Engineering*, June 12-13. IEEE Computer Society Press, 1996.

[49] H. P. Mckean. Nagumo's equation. *Advances in Mathematics*, 4:209–223, 1970.

[50] C. Mitchell and D. Schaeffer. A two-current model for the dynamics of cardiac membrane. *Bulletin of Mathematical Biology*, 65:767–793, 2003.

[51] G. Moe, W. Rheinboldt, and J. Abildskov. A computer model of atrial fibrillation. *Am Heart J*, 67:200–220, 1964.

[52] M. Osborne and G. Smyth. A modified Prony algorithm for exponential function fitting. *SIAM J. Sci. Comput.*, 16(1):119–138, 1995.

[53] V. Pavlovic, J. Rehg, T.-J. Cham, and K. Murphy. A dynamic bayesian network approach to figure tracking using learned dynamic models. In *Proc. of 7th IEEE Int. Conf. on Computer Vision*, 1999.

[54] L. S. Pontryagin. The asymptotic behaviour of systems of differential equations with a small parameter multiplying the highest derivatives. *Izv. Akad. Nauk SSSR, Ser. Mat.*, 21(5):107–155, 1957.

[55] R. D. Simitev and V. N. Biktashev. Conditions for propagation and block of excitation in an asymptotic model of atrial tissue. *Biophysical Journal*, 90:2258–2269, 2006.

[56] A. Singh and J. Hespanha. Models for generegulatory networks using polynomial stochastic hybrid systems. In *CDC05*, 2005.

[57] R. Suckley and V. N. Biktashev. Comparison of asymptotics of heart and nerve excitability. *Physical Review E*, 68, 2003.

[58] A. N. Tikhonov. Systems of differential equations, containing small parameters at the derivatives. *Mat. Sbornik*, 31(3):575–586, 1952.

[59] M. True, E. Entcheva, S. A. Smolka, P. Ye, and R. Grosu. Efficient event-driven simulation of excitable hybrid automata. In *Proceedings of EMBC*, 2006.

[60] P. Varaiya. Smart cars on smart roads: problems of control. *IEEE Trans. Automatic Control*, 38(2), 1993.

[61] R. Vidal, S. Soatto, Y. Ma, and S. Sastry. An algebraic geometric approach to the identification of a class of linear hybrid systems. In *Proc. of 42nd IEEE Conf. on Decision and Control*, 2003.

[62] P. Ye, E. Entcheva, R. Grosu, and S. A. Smolka. Efficient modeling of excitable cells using hybrid automata. In *Computational Methods in Systems Biology*, 2005.

[63] P. Ye, E. Entcheva, S. Smolka, and R. Grosu. A cycle-linear hybrid-automata model for excitable cells. *IET Systems Biology*, 2(1):24–32, Jan 2008.

[64] S. Yovine. Kronos: A verification tool for real-time systems. *International Journal of Software Tools for Technology Transfer*, 1:123–133, 1997.

[65] J. Zeng and Y. Rudy. Early afterdepolarizations in cardiac myocytes:mechanism and rate dependence. *Biophysical J.*, 68:949–964, 1995.

Appendix

```
dimension:  2; /* system dimension=2:  x[0]=clock, x[1]=voltage
*/
constants:  /* constant parameters in the description */
a0 = 0.2, /* a_0 */
a1 = 3.0, /* a_1 */
a2 = -0.7, /* a_2 */
VT = 5.7, /* Threshold V_T */
VO = 106, /* Threshold V_0 */
Ist = 11 /* Stimulus current I_st */;

initloc:  0;/* Initially the system is in mode Stimulated */
initset:  type rectangle
0.0 0.0,/* time is 0 */
0.0 0.01; /* voltage is 0 */

/* Mode Stimulated */
location:  0; /* dynamics Ẋ = AX + BU  */
matrixA:/* matrix A */
0.0 0.0,
0.0 [a0];
scalB: 1.0; /* B = 1.0 */
inputset:  /* the input is a rectangle area */
type rectangle
1.0 1.4, /* rate for clock x is ranging between 1.0 and 1.4 */
0.0 [Ist]; /* the current is ranging from 0 to 11*/
stayset:  /* Invariant in mode Stimulated */
type rectangle
0.0 0.501,/* system has to leave this mode after time x > 0.501 */
0.0 100.0; /* no specific requirements for voltage */
transition:  /* outgoing transitions */
label go01:/* transition to mode Rising */
```

```
if in guard:
type rectangle
0.5 0.501,/* at the time when stimulation ends */
[VT] [VO];/* voltage is greater than V_T */
goto 1;
label go02:  /* transition to mode Falling */
if in guard:
type rectangle
0.5 0.501, /* at the time when stimulation ends */
0.0 [VT]; /* voltage is smaller than V_T*/
goto 2;
/* Mode Rising */
location:  1;
matrixA:
0.0 0.0,
0.0 [a1];
scalB: 1.0;
inputset:  type convex_vert
1.0 0.0;
transition:
label go12:  /* transition to mode Falling */
if in
guard:  type rectangle
0.0 5.0, /* no specific requirements for time */
[VO] 1000;/* voltage is greater than V_0 */
goto 2;

/* Mode Falling */
location:  2;
matrixA:
0.0 0.0,
0.0 [a2];
scalB: 1.0;
```

```
inputset:  type convex_vert
1.0 0.0;
transition:
;

limits:  /* beyond this area, no analysis will be carried out.*/
x[0] <= 5.0 and
x[0] >= 0.0 and
x[1] <= 120.0 and
x[1] >= -1.0
```